INTERNATIONAL ATOMIC ENERGY AGENCY
UNITED NATIONS EDUCATIONAL, SCIENTIFIC AND CULTURAL ORGANIZATION
INTERNATIONAL CENTRE FOR THEORETICAL PHYSICS
I.C.T.P., P.O. BOX 586, 34100 TRIESTE, ITALY, CABLE: CENTRATOM TRIESTE

SMR/455 - 15

EXPERIMENTAL WORKSHOP ON HIGH TEMPERATURE SUPERCONDUCTORS & RELATED MATERIALS (BASIC ACTIVITIES)

12 - 30 MARCH 1990

JOSEPHSON EFFECT

ROBERTO CRISTIANO

Istituto di Cibernetica
Consiglio Nazionale delle Ricerche
Via Toiano, 6
Arco Felice (Napoli)
Italy

These are preliminary lecture notes, intended only for distribution to participants.

Josephson Effect

Roberto Cristiano - Istituto Cibernetica CNR
Arco Felice Naples Italy

Low T_c Superc.

- Basic Concepts and Equations
- Different Structures
- Tunnel Junctions : RSJ Model
- Temperature depend. of I_c
- Junction in a magnetic field
- SQUID

High-T_c Superc.

- Various Structures Realized
- dV/dI vs V curves Tunneling Spectroscopy
- Josephson Behaviour , SQUID Config.
- Conclusions

Applications

- Memory elements, logic devices
- Microwave Detectors and Generators
- Magnetometers in SQUID config.
- Voltage Standard
- Nuclear Radiation Detectors

t = thickness of the oxide

t very large

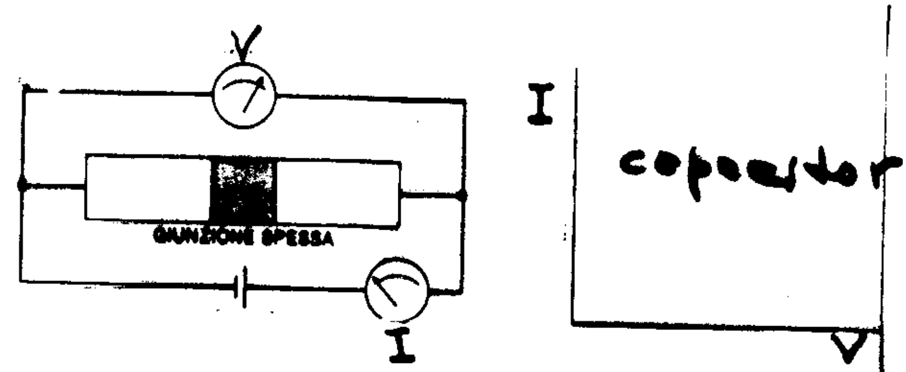

$t \sim 50\text{-}100$ Å
$T > T_c$

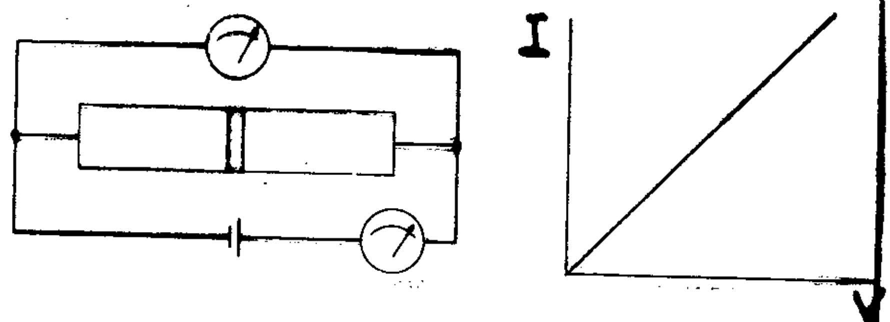

$t \sim 50\text{-}100$ Å
$T < T_c$

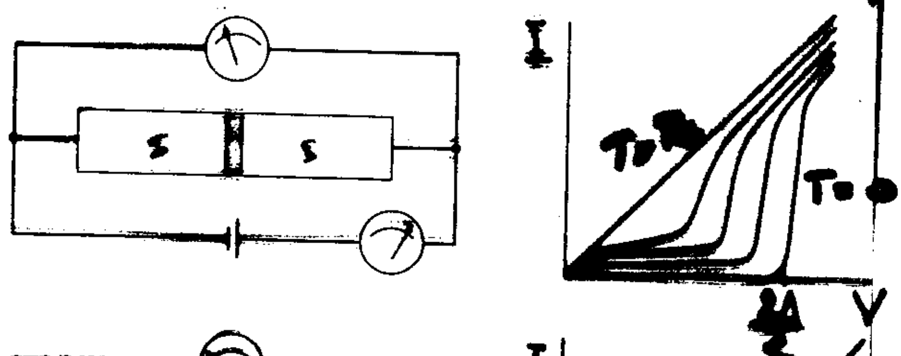

$t \sim 10\text{-}20$ Å
$T < T_c$

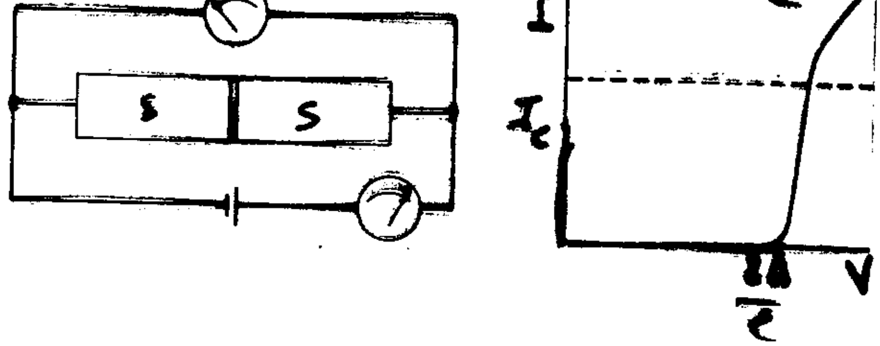

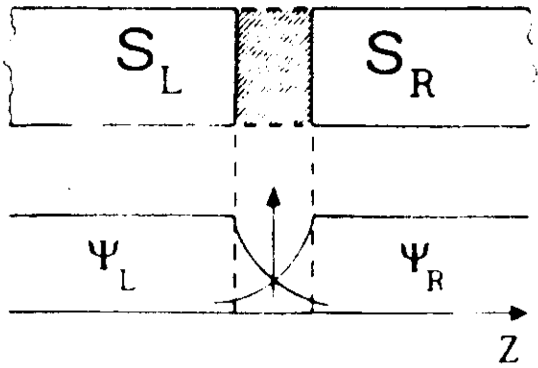

Figure 1.5 Schematic of a Josephson junction. S_L and S_R are the left and right superconductors. Ψ_L and Ψ_R are the left and right pair wavefunctions.

$$\Psi_{L,R} = \rho_{L,R}^{1/2} e^{i\varphi_{L,R}}$$

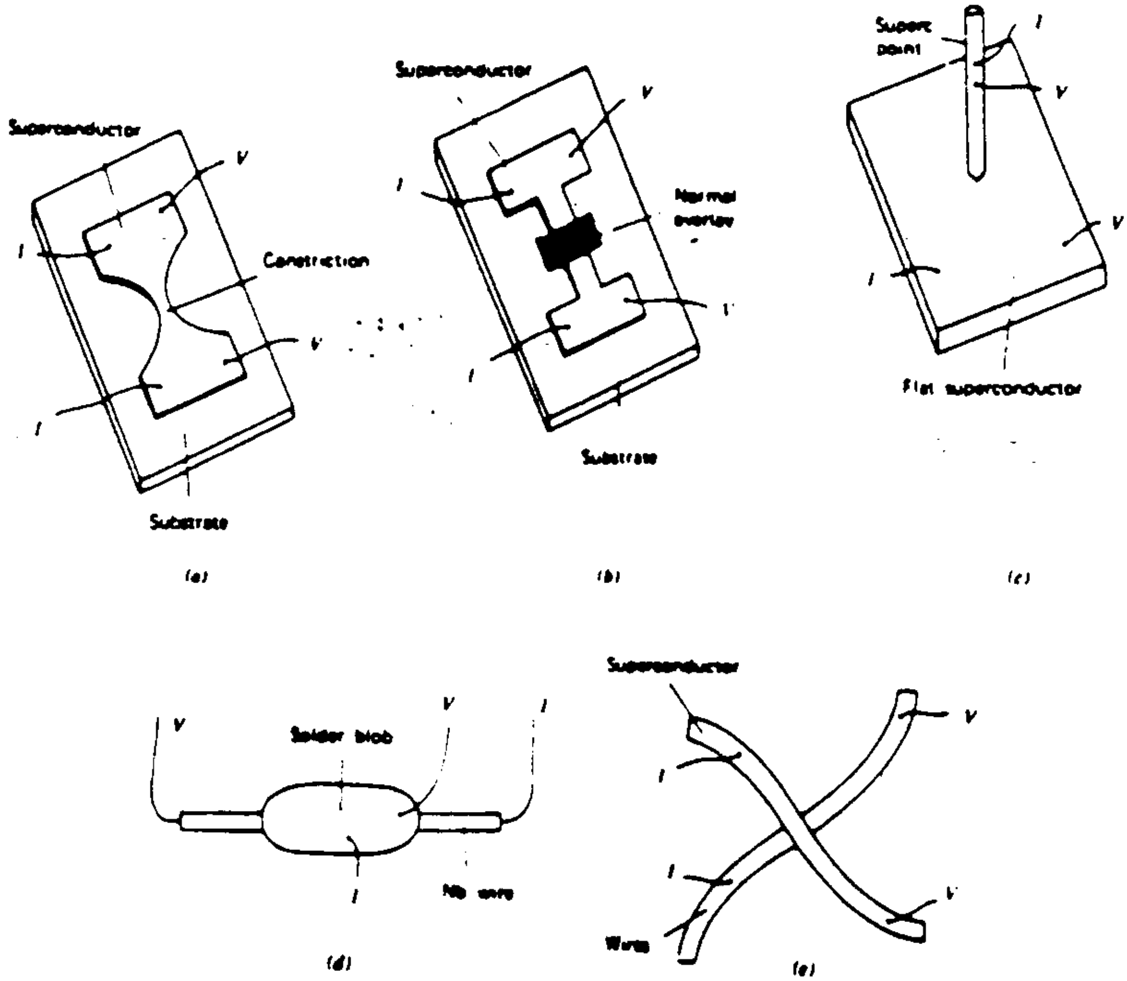

Fig. 5 - Configurazione di superconduttori debolmente accoppiati. a) "Dayem bridge"; b) bridge ad effetto di prossimità; c) punto contatto; d) tipo "Clarke"; e) link mediante fili incrociati.

Tunnel Junctions

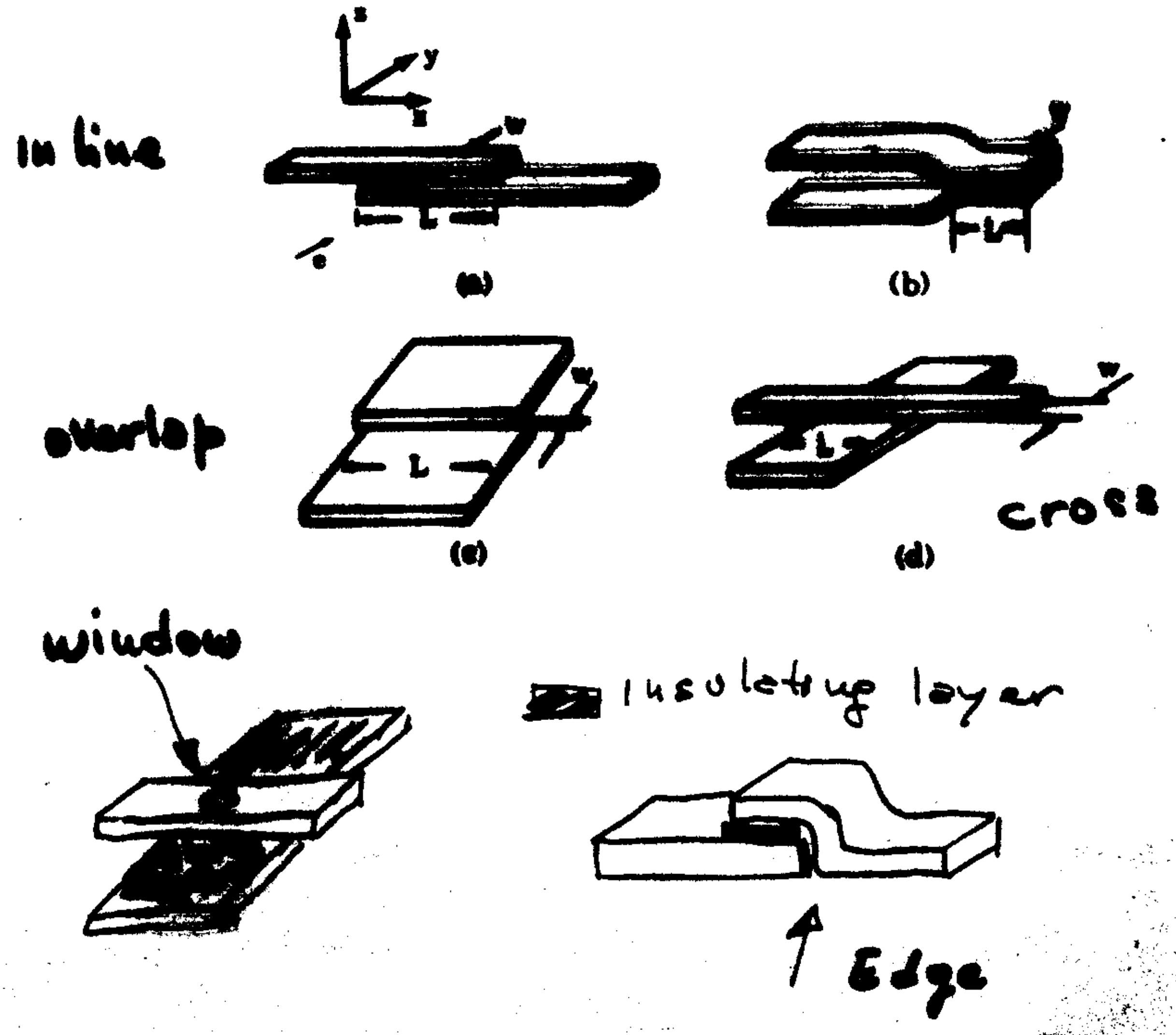

TECHNOLOGIES INVOLVED IN THE FABRICATION OF LOW T_c JOSEPHSON JUNCTION DEVICES

- VACUUM DEPOSITION OF THIN FILMS
- ULTRA VACUUM PUMPING
- OXIDE BARRIERS
- JUNCTION PATTERNING

• **ALL REFRACTORY, ARTIFICIAL BARRIER JUNCTIONS FABRICATION**

"Nb - AlO_x - Nb"

Feynmann model

Base states for the two superconductors: $|R\rangle, |L\rangle$

$$|\psi_L|^2 = \rho_L \quad ; \quad |\psi_R|^2 = \rho_R$$

State vector for the system $|\psi\rangle = \psi_R|R\rangle + \psi_L|L\rangle$

with a time-evolution given by the S. eq.

$$i\hbar \frac{\partial|\psi\rangle}{\partial t} = H|\psi\rangle \qquad H = H_L + H_R + H_T$$

$$H_L = E_L|L\rangle\langle L| \,,\quad H_R = E_R|R\rangle\langle R| \,,\quad H_T = K\left[|L\rangle\langle R| + |R\rangle\langle L|\right]$$

E_L, E_R ground state energies of L and R –

projecting on the two base states:

$$i\hbar \frac{\partial \psi_R}{\partial t} = E_R\psi_R + K\psi_L$$

$$i\hbar \frac{\partial \psi_L}{\partial t} = E_L\psi_L + K\psi_R$$

$$E_L - E_R = 2eV$$

$$\boxed{\begin{aligned} i\hbar \frac{\partial \psi_R}{\partial t} &= eV\psi_R + K\psi_L \\ i\hbar \frac{\partial \psi_L}{\partial t} &= -eV\psi_L + K\psi_R \end{aligned}} \longrightarrow$$

$$\begin{cases} \dfrac{\partial \rho_L}{\partial t} = \dfrac{2}{\hbar} K\sqrt{\rho_L\rho_R}\,\sin\varphi \\[2mm] \dfrac{\partial \rho_R}{\partial t} = -\dfrac{2}{\hbar} K\sqrt{\rho_L\rho_R}\,\sin\varphi \\[2mm] \dfrac{\partial \varphi_L}{\partial t} = \dfrac{K}{\hbar}\sqrt{\dfrac{\rho_L}{\rho_R}}\cos\varphi - \dfrac{eV}{\hbar} \\[2mm] \dfrac{\partial \varphi_R}{\partial t} = \dfrac{K}{\hbar}\sqrt{\dfrac{\rho_L}{\rho_R}}\cos\varphi + \dfrac{eV}{\hbar} \end{cases}$$

since $\varphi = \varphi_L - \varphi_R$ ←

and $\dfrac{\partial \rho_L}{\partial t} = -\dfrac{\partial \rho_R}{\partial t} \equiv J$

Josephson Eqs.

$$J = \frac{2k}{\hbar} \sqrt{\rho_L \rho_R} \sin\varphi \equiv J_c \sin\varphi$$

$$\frac{\partial \varphi}{\partial t} = \frac{2e}{\hbar} V$$

1) $J < J_c$ $\qquad \varphi = \arcsin J/J_c = \text{const} \neq 0$

$$\frac{\partial \varphi}{\partial t} = 0 \Rightarrow V = 0$$

d.c. Josephson Effect

2) $V \neq 0$ but const, $V(t) = V_0$

$$\varphi = \frac{2e}{\hbar} V_0 t + \alpha \Rightarrow J = J_c \sin\left(\frac{2e}{\hbar} V_0 t + \alpha\right)$$

$$= J_c \sin(\omega_J t + \alpha)$$

$$\omega_J = \frac{2e}{\hbar} V_0 \sim 484 \text{ MHz}/\mu V$$

a.c. Josephson Effect

gure 1.7 Typical voltage-current characteristic for a Sn-Sn$_x$O$_y$-Sn Josephson junction at $T = 1.52$
Horizontal scale: 0.5 mV/div; vertical scale: 2 mA/div

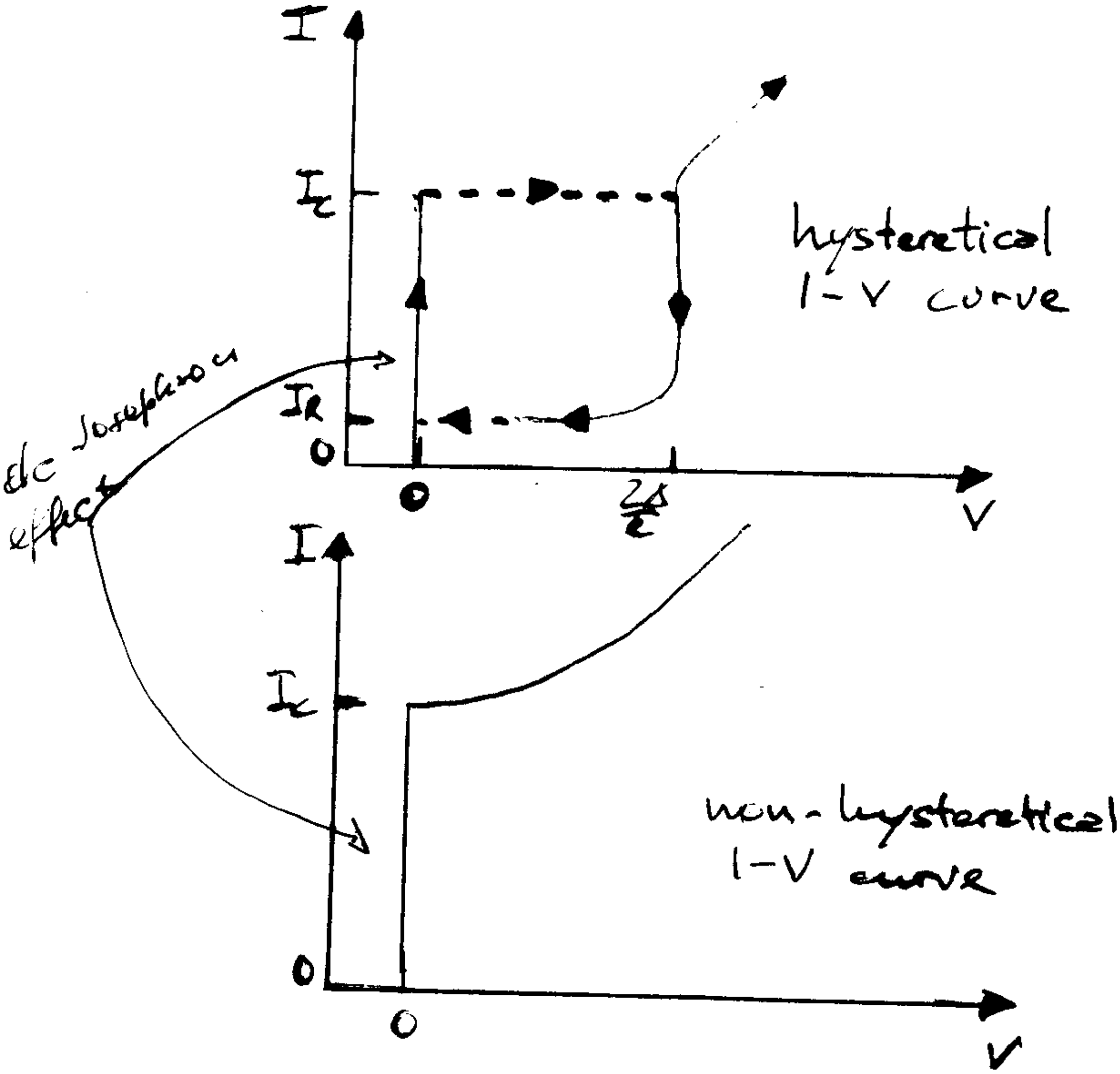

$$J = J_c \sin\left(\frac{2e}{\hbar} V t + \frac{2e}{\hbar} d B_e x + \varphi_0\right)$$

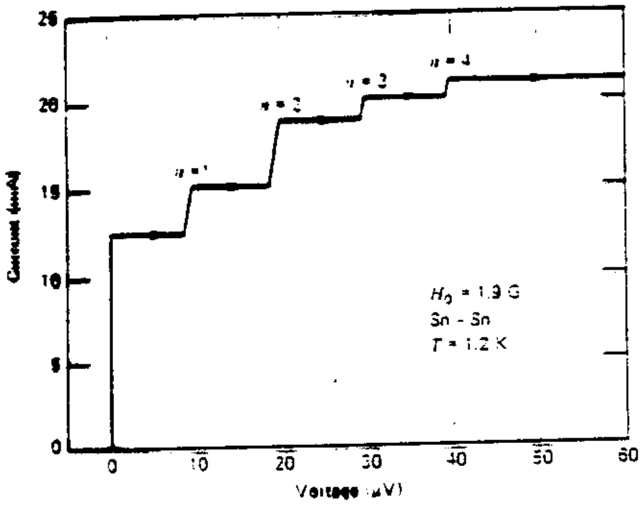

A typical V-I curve for an Sn-SnO$_x$-Sn junction showing self-steps in the presence of a magnetic field. The curve is traced using a variable d.c. current bias. (After Langenberg, Scalapino, and Taylor 1966.)

$$\frac{2e V_n}{\hbar} = \frac{n \pi \bar{c}}{L} = \omega_0$$

$$V_n = \frac{\hbar}{2e}\omega_n = \frac{\hbar}{2e}\frac{\bar{c}}{2L}n$$

$$\omega_0 = \omega_n \quad , \quad k_0 = k_n$$

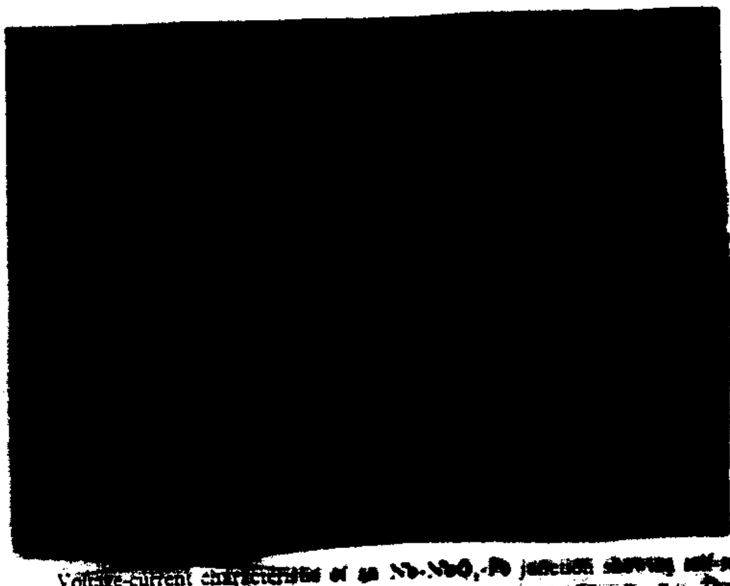

Voltage-current characteristic of an Nb-NbO$_x$-Pb junction showing self-steps in an applied magnetic field. Vertical scale 0.1 mA/div; horizontal scale in arbitrary units. The curve has been traced using a variable d.c. bias overimposed on a low frequency a.c. bias. The picture was taken by multiple exposure.

1) Microwave Induced Steps — **Shapiro Steps**

Microwave Receivers

2) Self-Induced steps

a) Small Junctions → External Magnetic Field must be applied

$L, W \ll \lambda_J$

Fiske Steps

b) Long Junctions – Self Induced Field, no external Field necessary

$L, W > \lambda_J$

Zero-Field Steps

→ Microwave Generators

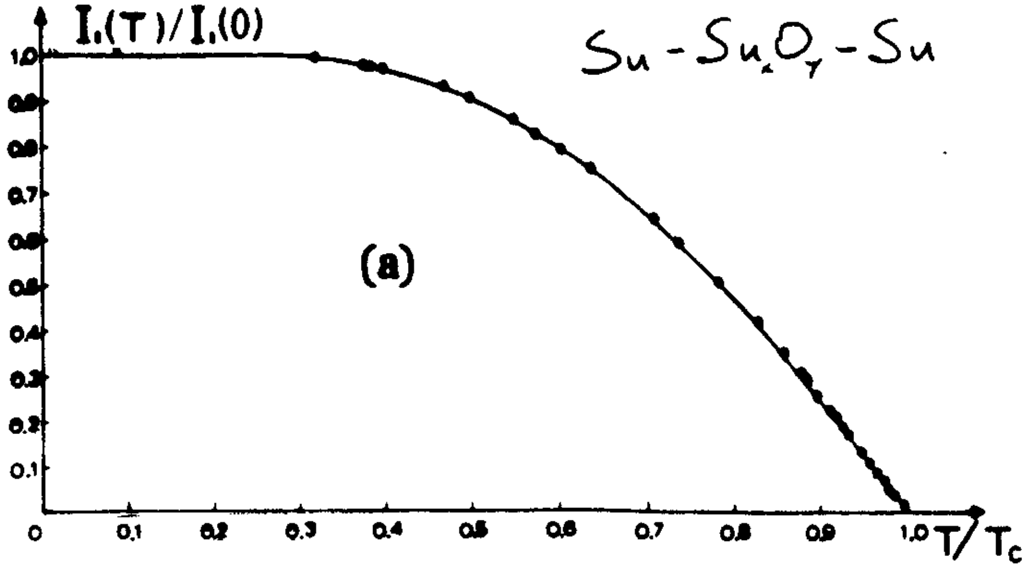

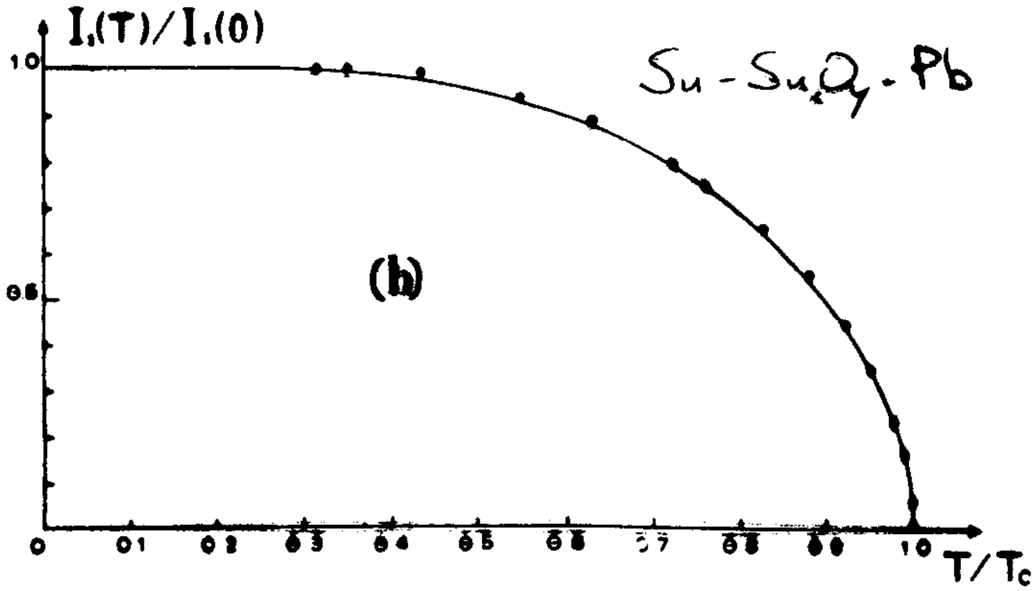

Figure 3.2 Temperature dependence of the maximum (d.c.) Josephson current. (*a*) Sn-SnO$_x$-Sn junction; (*b*) Sn-SnO$_x$-Pb junction. The experimental data (solid circles) are compared with the theoretical curves (solid lines) calculated using the Ambegaokar and Baratoff results. The maximum error in the data is smaller than the dimensions of the solid circles. (After Balsamo et al. 1974.)

$\Delta_L = \Delta_R$ $$I_c(T=0) = \frac{\pi}{2}\frac{\Delta(0)}{e R_N}$$

$$I_c(T) = \frac{\pi}{2}\frac{\Delta(T)}{R_N}\tanh\left(\frac{\Delta(T)}{2kT}\right)$$

Ambegaokar, Baratoff

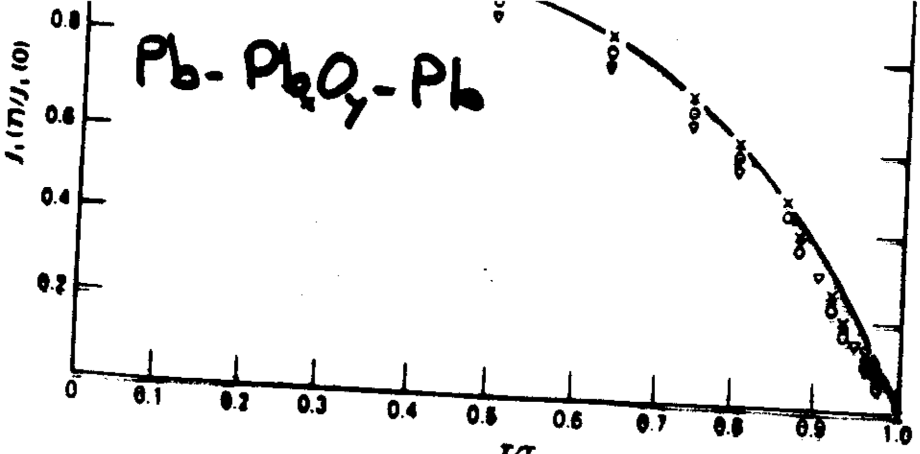

Figure 3.5 Plot of the normalized d.c. Josephson current, $I_1(T)/I_1(0)$ vs. reduced temperature T/T_c. The solid line is the experimental temperature variation observed for Pb-Pb junctions. The crosses are the strong coupling values calculated from (3.3.2). The solid triangles are the predictions of (3.2.10) using the B.C.S. $\Delta(T)$, while the solid circles are the result of putting the strong coupling $\Delta(T)$ into (3.2.10). (After Lim et al. 1970.)

Strong-Coupling supercond. (Pb)!
(Complex energy dependent gap)

solid line experiment

+ Strong Coupl. Predict.

Δ BCS Gap in BCS $I_c(T)$

Magnetic Impurities

× t_c

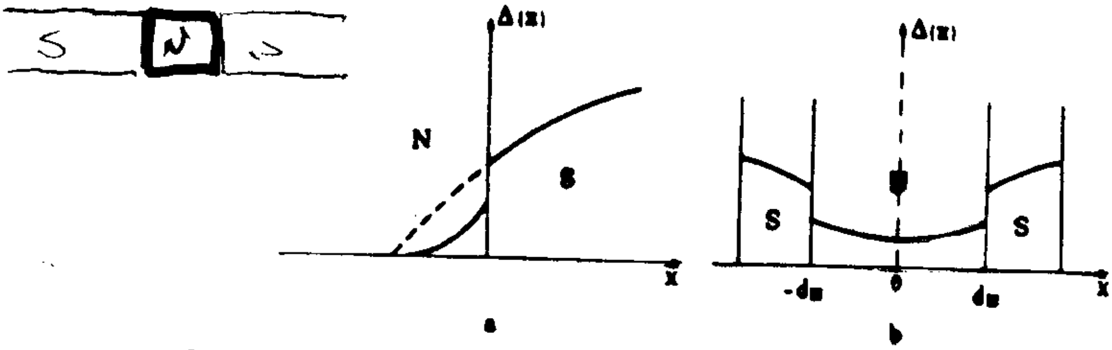

Figure 7.1 Qualitative sketch of the order parameter behavior at temperature close to the critical (see, for instance De Gennes 1964.) (*a*) *N-S* system; (*b*) *S-N-S* junction.

Proximity effect: Reduction of superc. properties of S due to the normal, and conversely a penetration of supercond. prop. in the normal at the interface.

Structures: S-N-S
S-S'-S $T_{cS'} < T_{cS}$
S-I-N-S Nb-Al-AlO-Nb
links

non hysteretical I-V curve

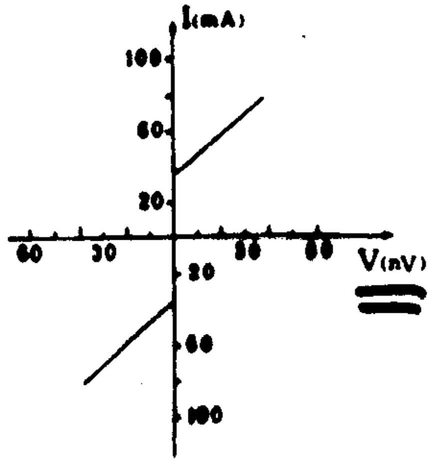

Figure 7.2
Voltage-current characteristics of an *SNS* junction at $T = 2.98$ K. Normal metal thickness-5520 Å; mean free path $l = 140$ Å. (After Clarke 1969.)

m. free path in normal

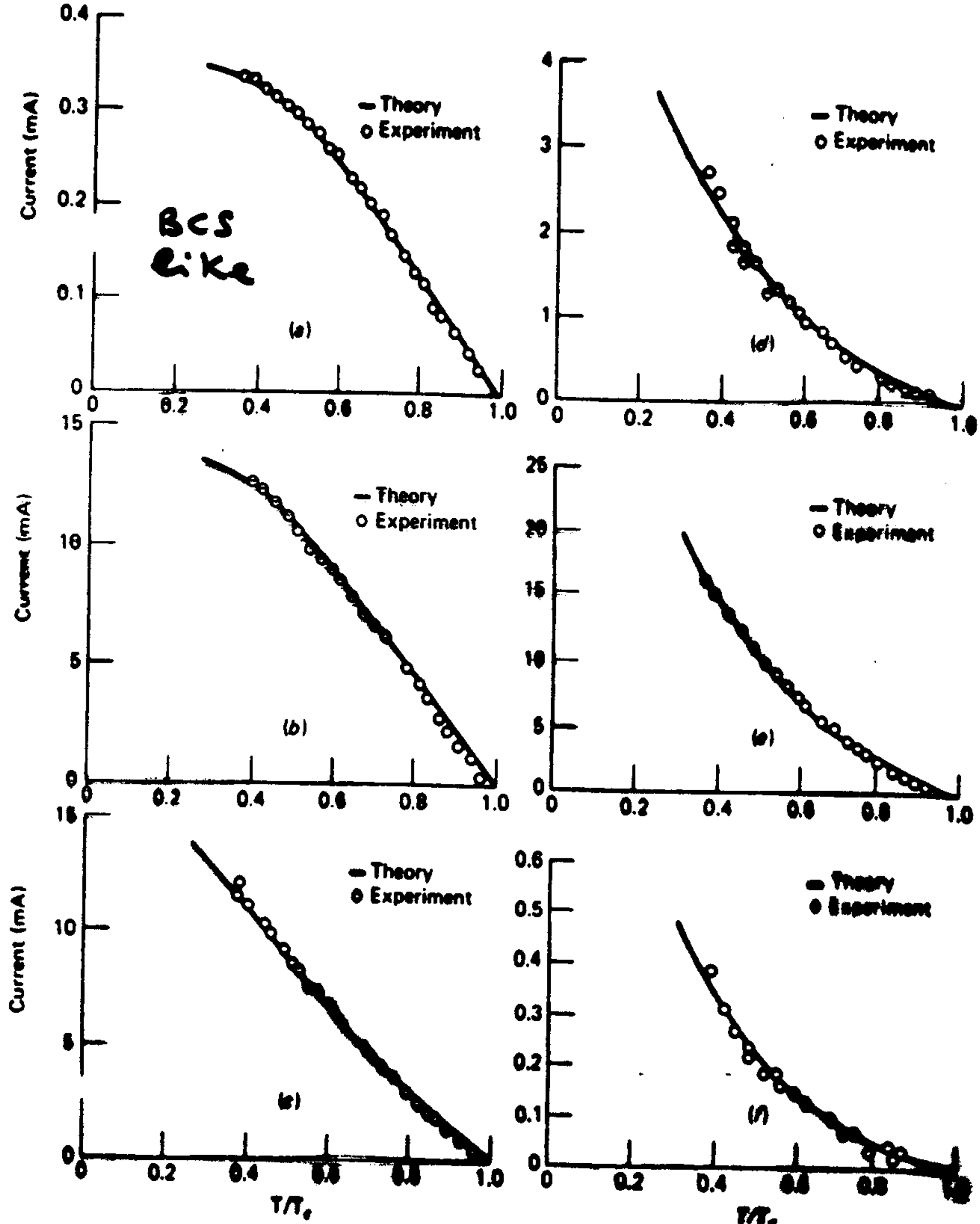

Figure 7.4 The Josephson current vs. reduced temperature for S-I-N-S structures. Data refer to Sn-Sn$_x$O$_y$-Zn-Sn structures. (a) $T_c = 3.68$ K, $d_N = 600$ Å, $l_N = 845$ Å. (b) $T_c = 3.60$ K, $d_N = 1800$ Å, $l_N = 1180$ Å. (c) $T_c = 3.34$ K, $d_N = 2400$ Å, $l_N = 916$ Å. (d) $T_c = 3.43$ K, $d_N = 3600$ Å, $l_N = 1130$ Å. (e) $T_c = 3.44$ K, $d_N = 3600$ Å, $l_N = 1110$ Å. (f) $T_c = 3.32$ K, $d_N = 3600$ Å, $l_N = 785$ Å. (After Rowell and Smith 1976.) (Reproduced by permission of the National Research Council

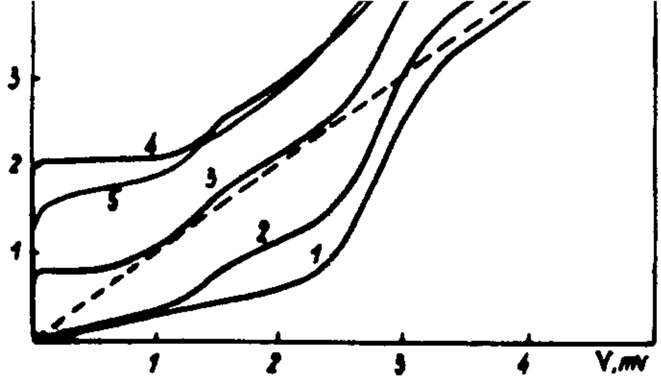

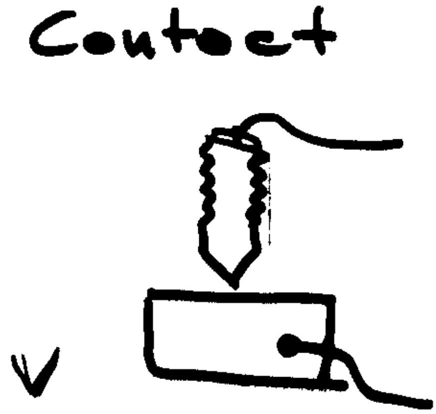

Fig. 1 : The modification of reduced I-V characteristics of Nb-Nbpoint contacts by successive adjustments. Contact resistances R, Ohm : 1 - 45 x 10^3, 2 - 15.5 x 10^3, 3 - 530, 4 - 8.4 (T=4.2 K). For curve 5 R=8.4 Ω and T=6.5 K. Dashed line is normal state I-V characteristic.

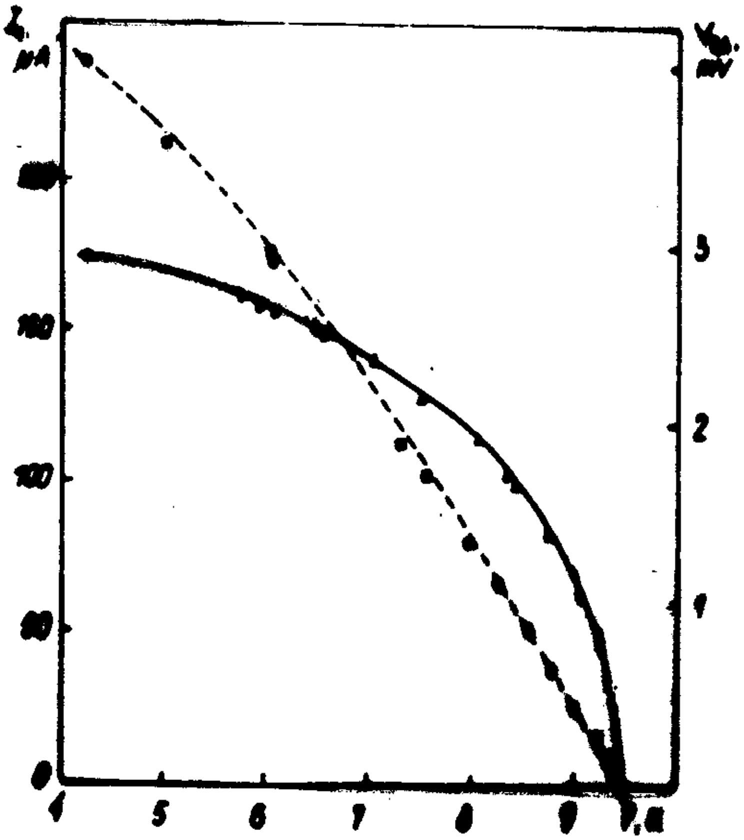

Fig. 2 : Temperature dependences of critical current I_c (■), gap structure V_Δ (▲) for contact with R=8.4 Ω. Solid line shows BCS dependence $2\Delta(T)$, dashed line is the theoretical dependence $I_c(T)$ for microbridges /5/.

Magnetic field depend of Ic

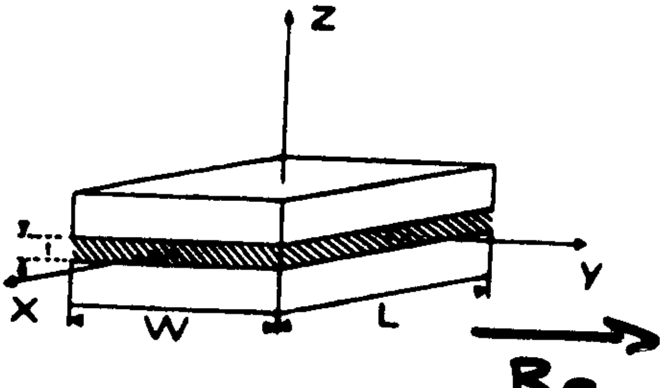

(a)

$$\begin{cases} \dfrac{\partial \varphi}{\partial x} = \dfrac{2e}{\hbar} d\, H_y \\[2ex] \dfrac{\partial \varphi}{\partial y} = \dfrac{2e}{\hbar} d\, H_x \end{cases} \qquad d = \lambda_L + \lambda_R + t_{ox}$$

$\underline{H}$ is the actual Magnetic field

$\underline{H} = \underline{H}_{ext} + \underline{H}_{ind}$

Josephson Junction Electrodynamics

Maxwell eq $\nabla \times \underline{H} = \frac{4\pi}{c} \underline{J} + \frac{1}{c} \frac{\partial \underline{D}}{\partial t}$

+

Josephson eqs

$$\Longrightarrow \boxed{\frac{\partial^2 \varphi}{\partial x^2} + \frac{\partial^2 \varphi}{\partial y^2} - \frac{1}{\bar{c}^2} \frac{\partial^2 \varphi}{\partial t^2} = \frac{1}{\lambda_J^2} \sin \varphi}$$

$$\lambda_J = \left(\frac{\hbar \bar{c}^2}{8\pi e d J_c} \right)^{1/2}$$

sine-Gordon Eq.

Stationary case $\frac{\partial \varphi}{\partial t} = 0$

1-dim and small φ

$$\frac{\partial^2 \varphi}{\partial x^2} = \frac{1}{\lambda_J^2} \varphi \qquad \varphi \sim \exp - \frac{x}{\lambda_J}$$

λ_J gives the distance where d.c. Josephson Current are confined to the edges of the junction

λ_J Josephson penetration depth

Small Junctions

$$L, W << \lambda_J$$

Uniform Current Distribution
Negligible Self-Induced Magnetic Field

Large Junctions

$$L \text{ and/or } W \gtrsim \lambda_J$$

Current typically confined at the edges
Relevant Self-Induced Effects.

$J = J_c \sin\varphi$

J is uniform in small junctions

J_c may be non-uniform in small junctions

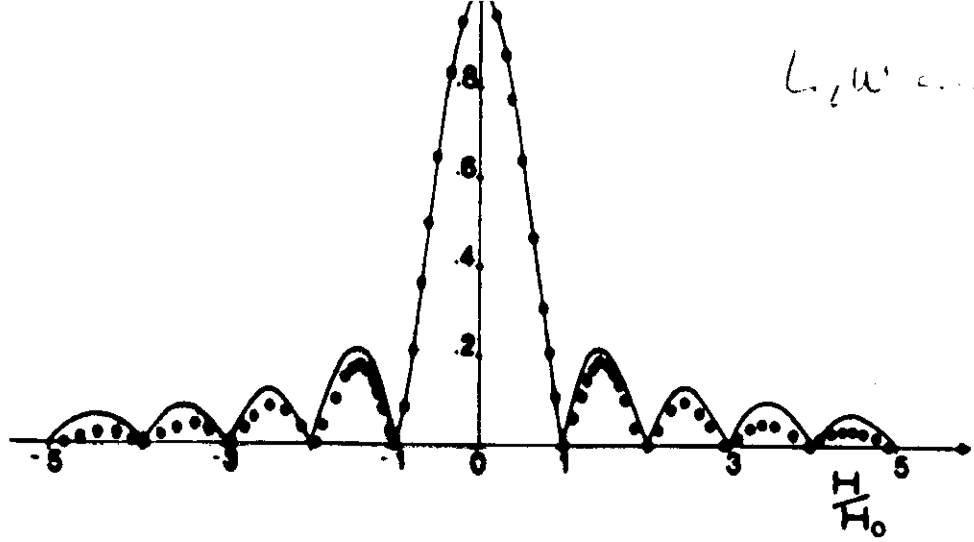

Figure 4.4 Magnetic field dependence of the maximum Josephson current I_1 for an Sn-Sn_xO_y-In rectangular junction. The circles are the experimental data; the solid line is the theoretical dependence computed from (4.3.1). (After Barone et al. 1976b.)

Fra... Pattern

$$J \ldots \left| \frac{\sin kL/2}{kL/2} \right|$$

where $k = \ldots$

$\Phi_{min} = n\,\Phi_0$ ... Magnetic ... quantum

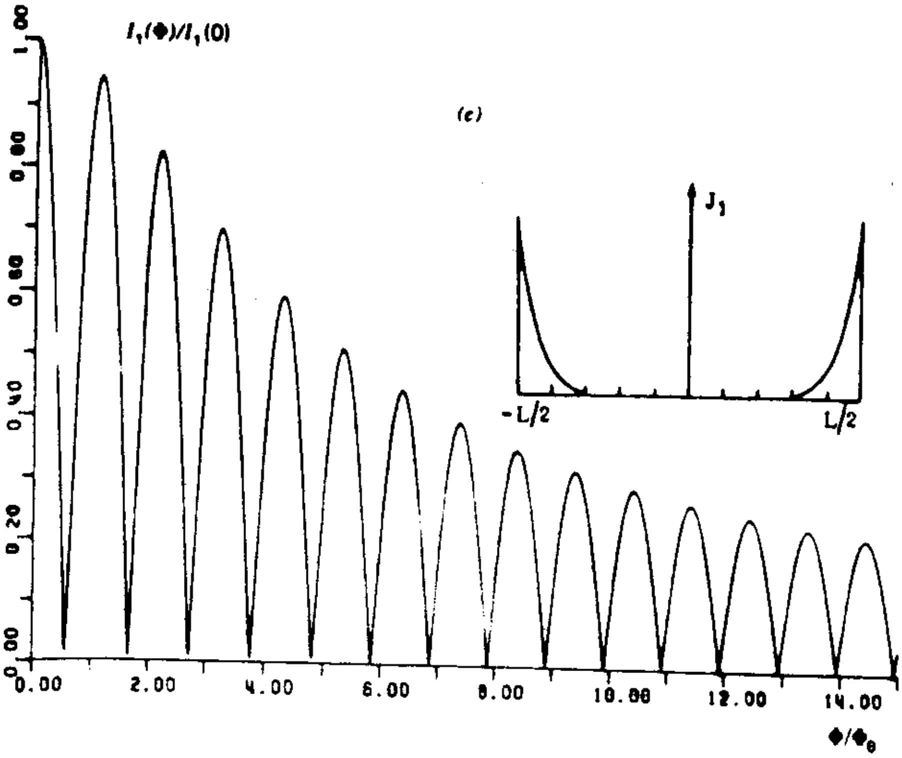

$I_1(\Phi)/I_1(0)$
(c)
J_1
-L/2
L/2
1.00
0.80
0.60
0.40
0.20
0.00
0.00
2.00
4.00
6.00
8.00
10.00
12.00
14.00
Φ/Φ_0

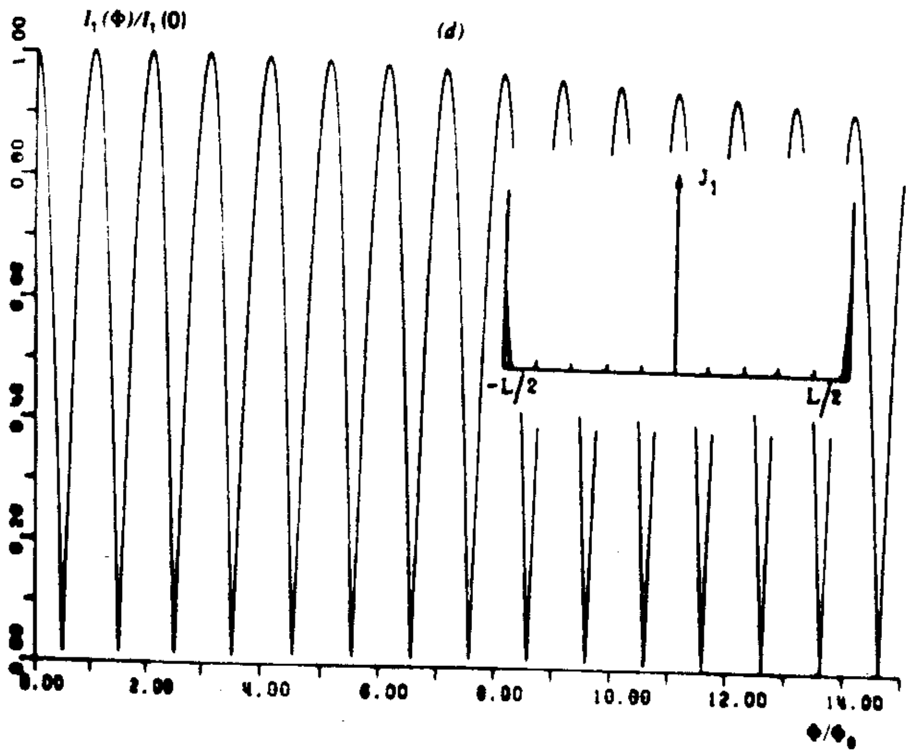

$I_1(\Phi)/I_1(0)$
(d)
J_1
-L/2
L/2
1.00
0.80
0.00
2.00
4.00
6.00
8.00
10.00
12.00
14.00
Φ/Φ_0

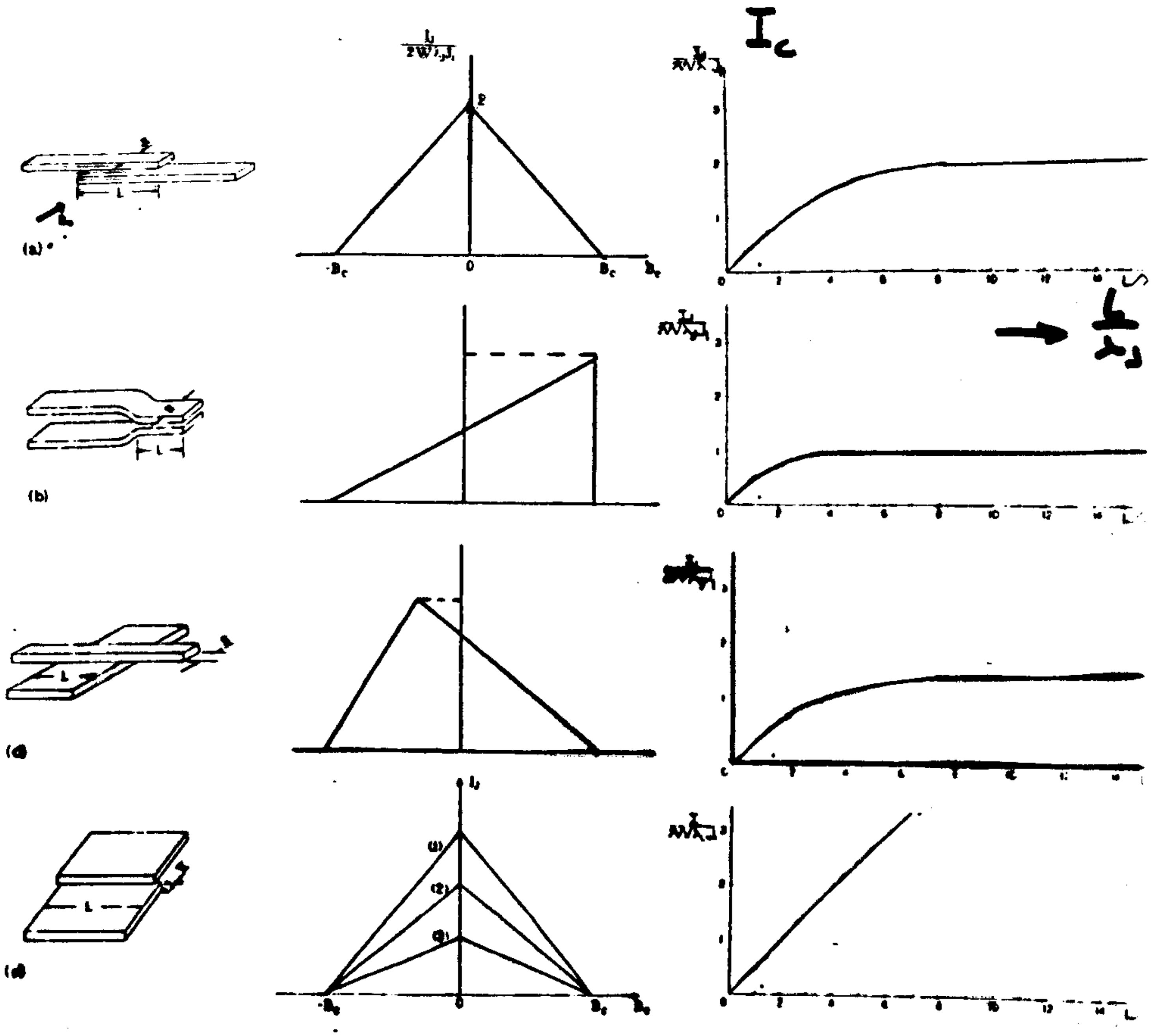

I_c
(a)
(b)
2
-B_c
0
B_c
B_e
(1)
(2)
(3)

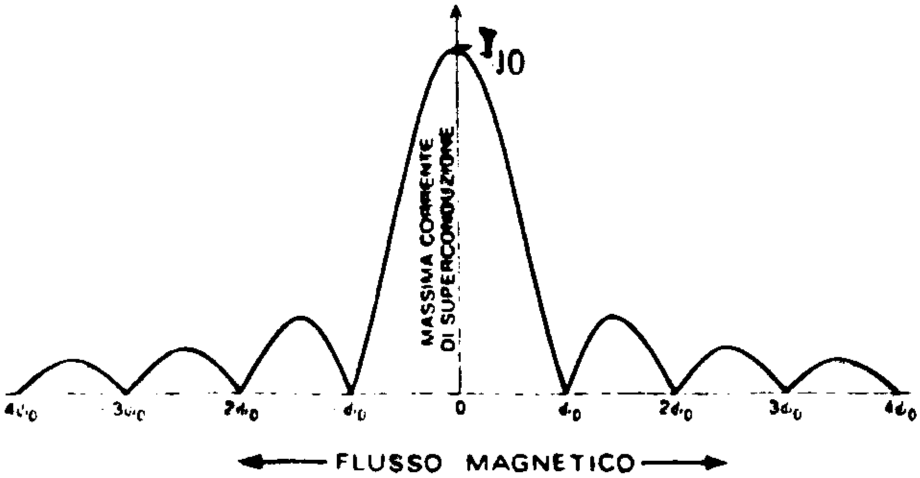
I J0
MASSIMA CORRENTE DI SUPERCONDUZIONE
0
FLUSSO MAGNETICO

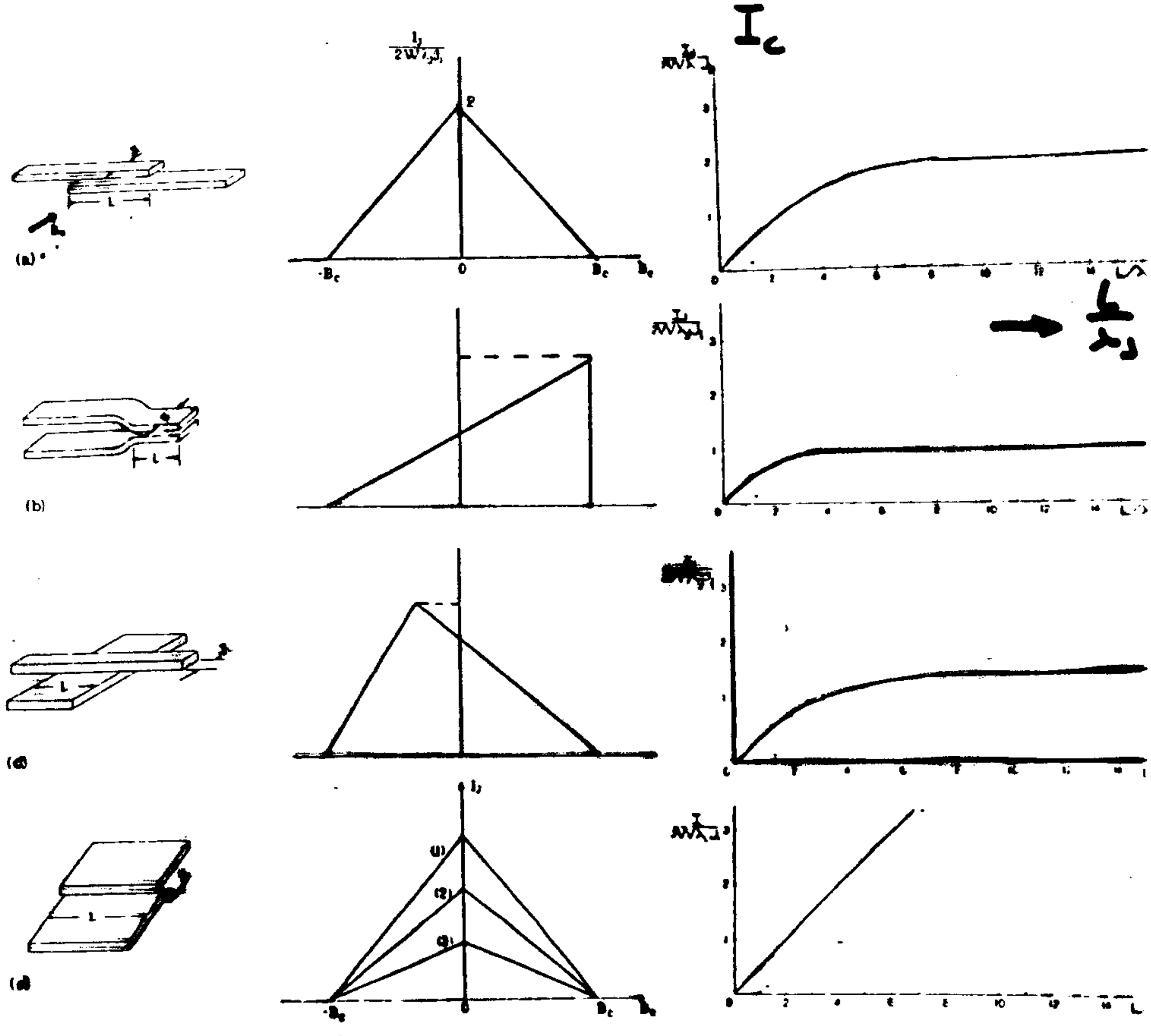
Ic
(a)
(b)
-Bc
0
Bc
Be
(1)
(2)
(3)

a

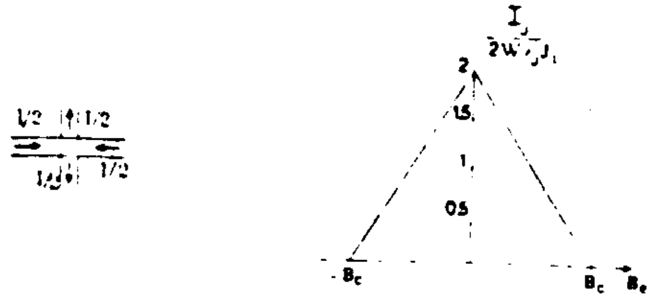

simmetrica

b

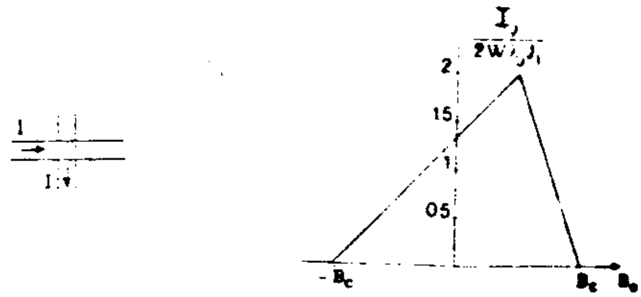

asimmetrica

c

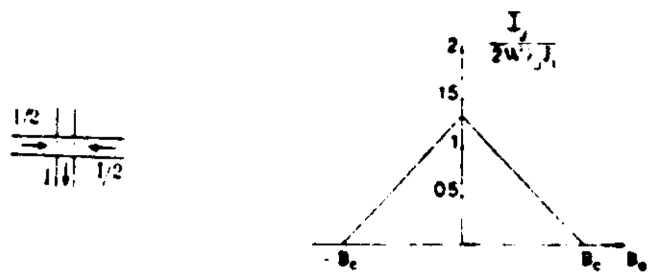

parzialmente
simmetrica

d

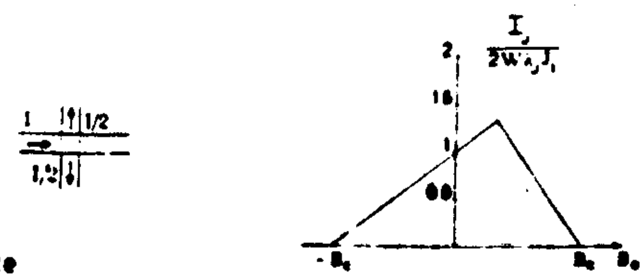

parzialmente
asimmetrica.

Effect of the bias current directions 5

Resistively Shunted Junction Model

Small Junctions $\quad L, W << \lambda_J$

$$\cancel{\frac{\partial^2\varphi}{\partial x^2}} + \cancel{\frac{\partial^2\varphi}{\partial z^2}} - \frac{1}{c}\frac{\partial^2\varphi}{\partial t} + k\frac{\partial\varphi}{\partial t} = \frac{1}{\lambda_J^2}\sin\varphi - I$$

dissipation $\qquad$ bias

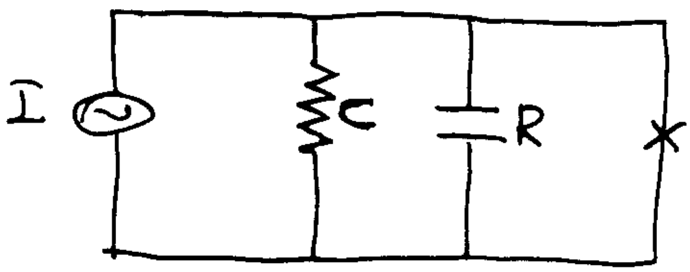

$I_J = I_c \sin\varphi$

$$C\frac{dV}{dt} + \frac{V}{R} + I_c \sin\varphi = I$$

$R = R(V, T)$ $\qquad$ if $I_c(H_e \neq 0) = 0$

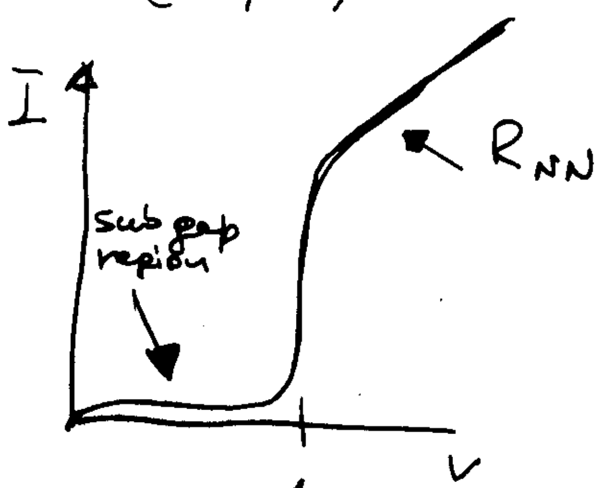

Gap voltage $= \frac{2\Delta}{e} \approx 2 \div 3$ mV

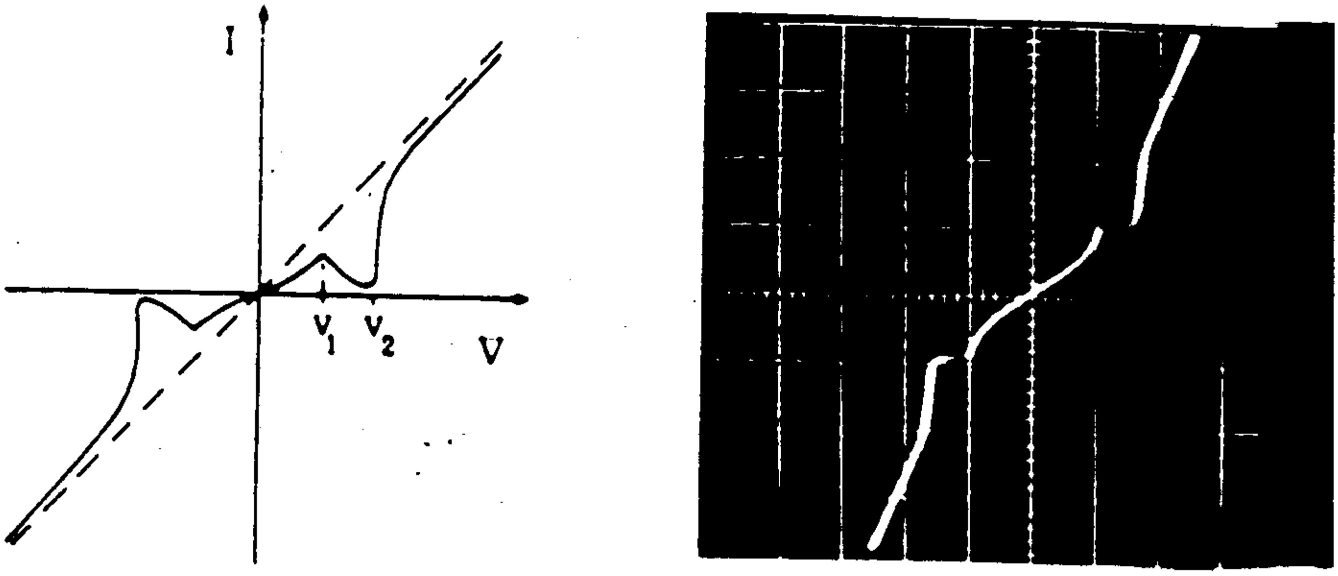

Fig. 1 - a) Caratteristica corrente-tensione di una giunzion costituita da superconduttori diversi. b) Caratteristica sperimental di una giunzione Sn-Sn_xO_y-Pb.
(Scala orizzontale 1mV/div; scala verticale 20 mA/div)

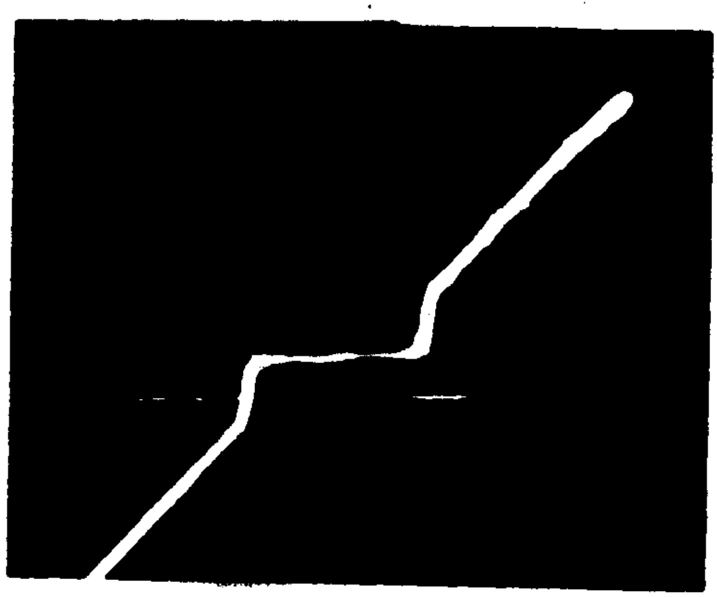

Fig. 2 - Caratteristica I-V per una giunzione costituita da due superconduttori uguali ($\Delta_1=\Delta_2$). Struttura Pb-Pb -
(Scala orizzontale 2mv/div; scala verticale 200µA/div)

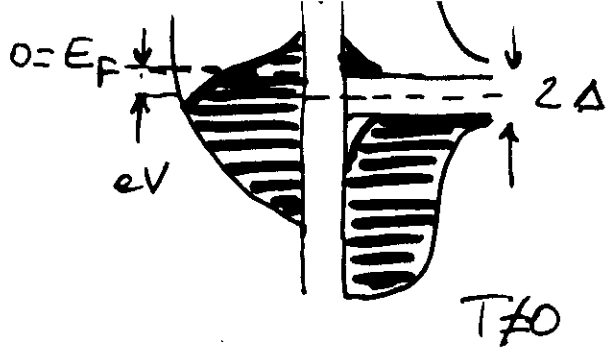

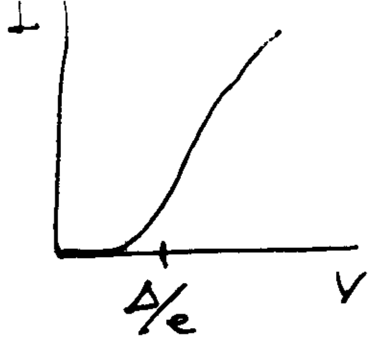

$T > T_c$

$$I_{L\to R} = T_{12}(E)\, N_L(E-eV)\, N_R(E)\, f(E-eV)\left[1-f(E)\right] dE$$

$$I_{R\to L} = T_{21}(E)\, N_L(E-eV)\, N_R(E)\, f(E)\left[1-f(E-eV)\right] dE$$

$$I_{NN} \sim A N_1(0) N_2(0) \int \underbrace{f(E-eV) - f(E)}_{\approx -eV \frac{df}{dE} \approx -eV\delta} dE$$

$$I_{NN} \sim A N_1 N_2 eV \qquad \sigma_{NN} = \frac{dI_{NN}}{dV} = A N_1 N_2 e$$

$$N_R(E) = N_N(E)\, n_s(E)$$

$$I_{NS} = A N_{1N} N_{2N} \int_0^{eV} n_s(E)\, dE$$

n_s superc. density of states

$$\sigma_{NS} = \frac{dI_N}{dV} = A N_{1N} N_{2N}\, n_s(eV)\, e$$

$$\boxed{\sigma_{NS} / \sigma_{NN} = n_s(V)}$$

Tunneling Spectroscopy

2 Junctions in a superc. Loop

1 Junction in a superc. Loop

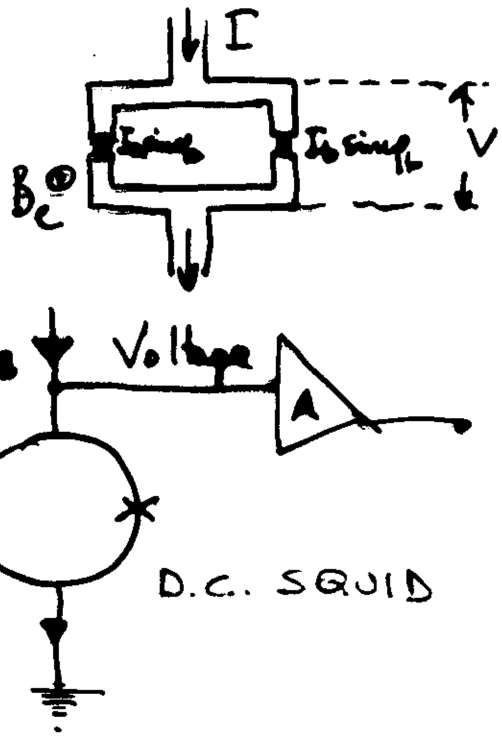

D.C. SQUID

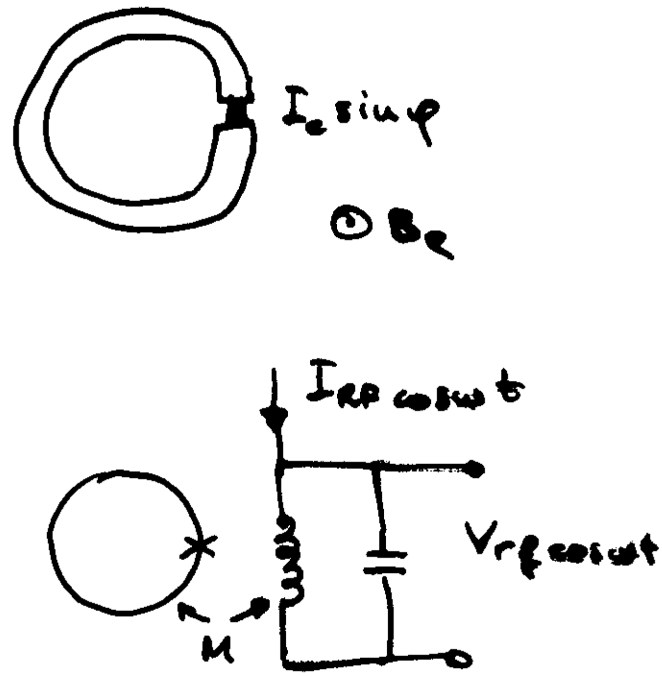

R.F. SQUID

Magnetometers

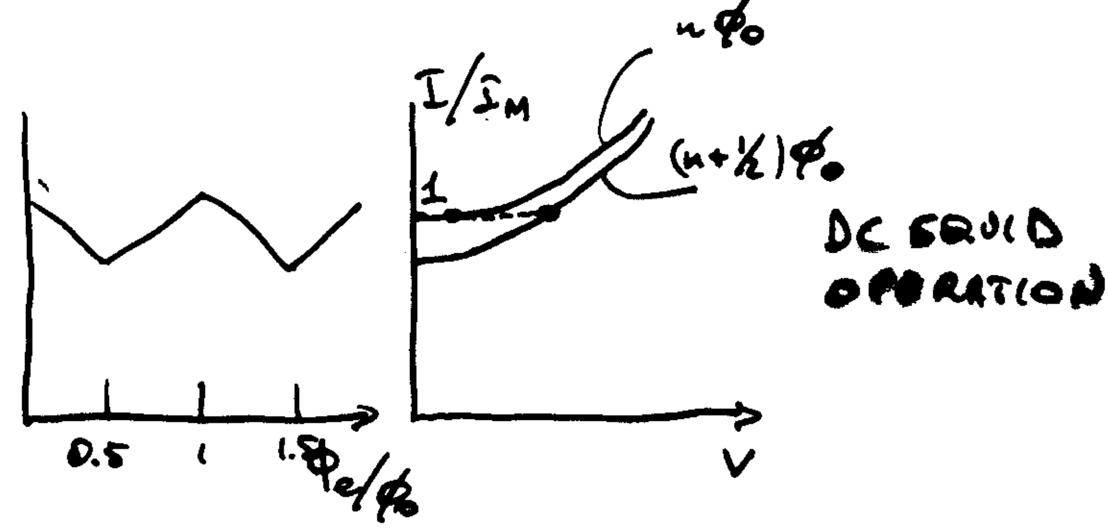

2 junctions interferometer
(dc SQUID)

$$I_M = 2 I_c \left| \frac{\sin \pi \Phi_J}{\pi \Phi_J} \right| \left| \cos \pi \phi_e \right|$$

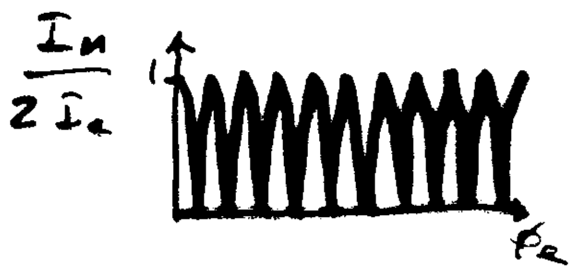

$I_a = I_b \quad \phi_J = 0$

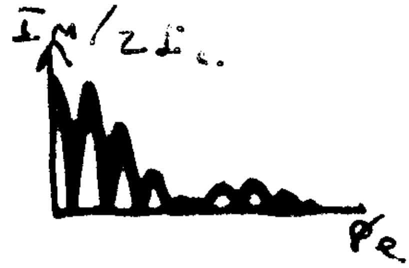

$I_a = I_b \quad \Phi_J = 0.2\, \phi_e$

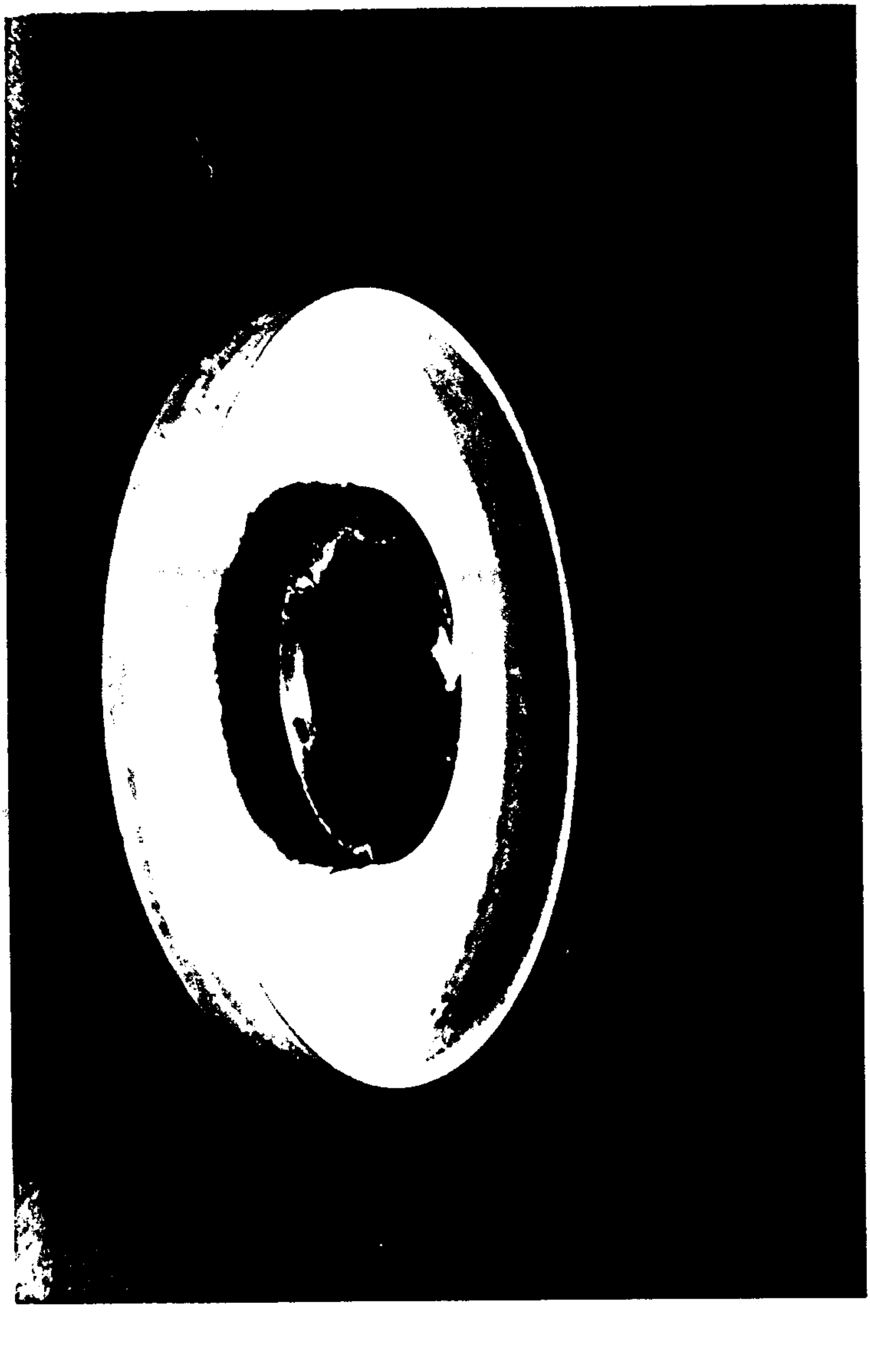

Junction Types

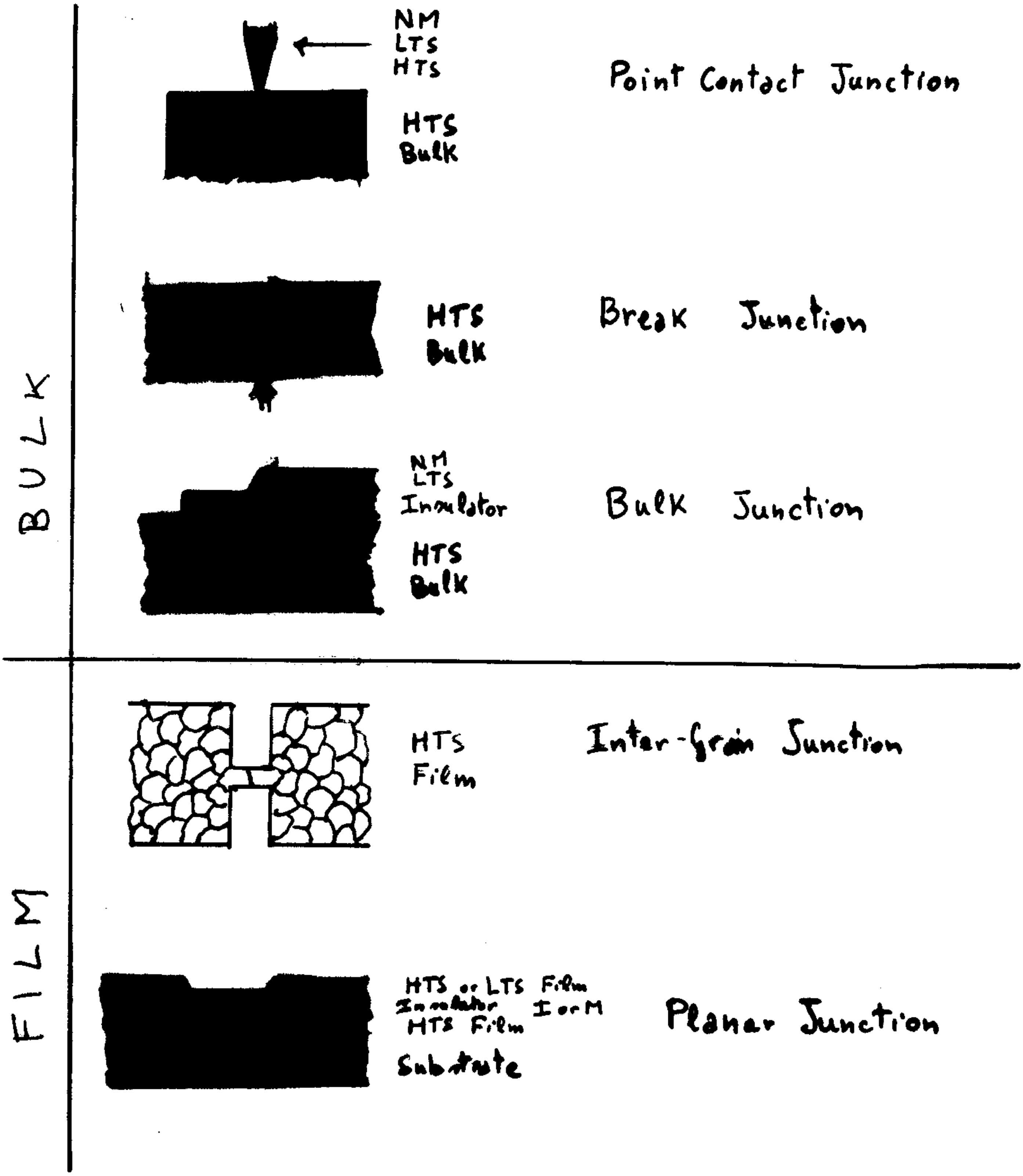

		Junction Type	Riproducibilit	Difficulty o Fabrication	Fully High Tc	Physical Prop Investigation	Device Applications
BULK		Point Contact	POOR	LOW	YES	(a) YES	NO
BULK		Break	POOR	LOW	YES	YES	NO
BULK	PLANAR	Bulk	MEDIUM	MEDIUM	NO	(b) NO	MAYBE
FILM	PLANAR	Intergrain	POOR	(c) MEDIUM	YES	(d) NO	(e) MAYBE
FILM	PLANAR	Sandwitch	GOOD	HIGH	YES	(f) NO	(g) YES

Remarks

a) In particulat STM studies on single crystals
b) Surface defradation
c) Worste wist good films
d) No control of grain interface
e) Only SQUIDs
f) Surface degradation. Possible study of proximity effect and anisotropy.
g) Require further improvement

Experimental set-up for point contact junctions

push-pull feedthrough
with a micrometrical screw

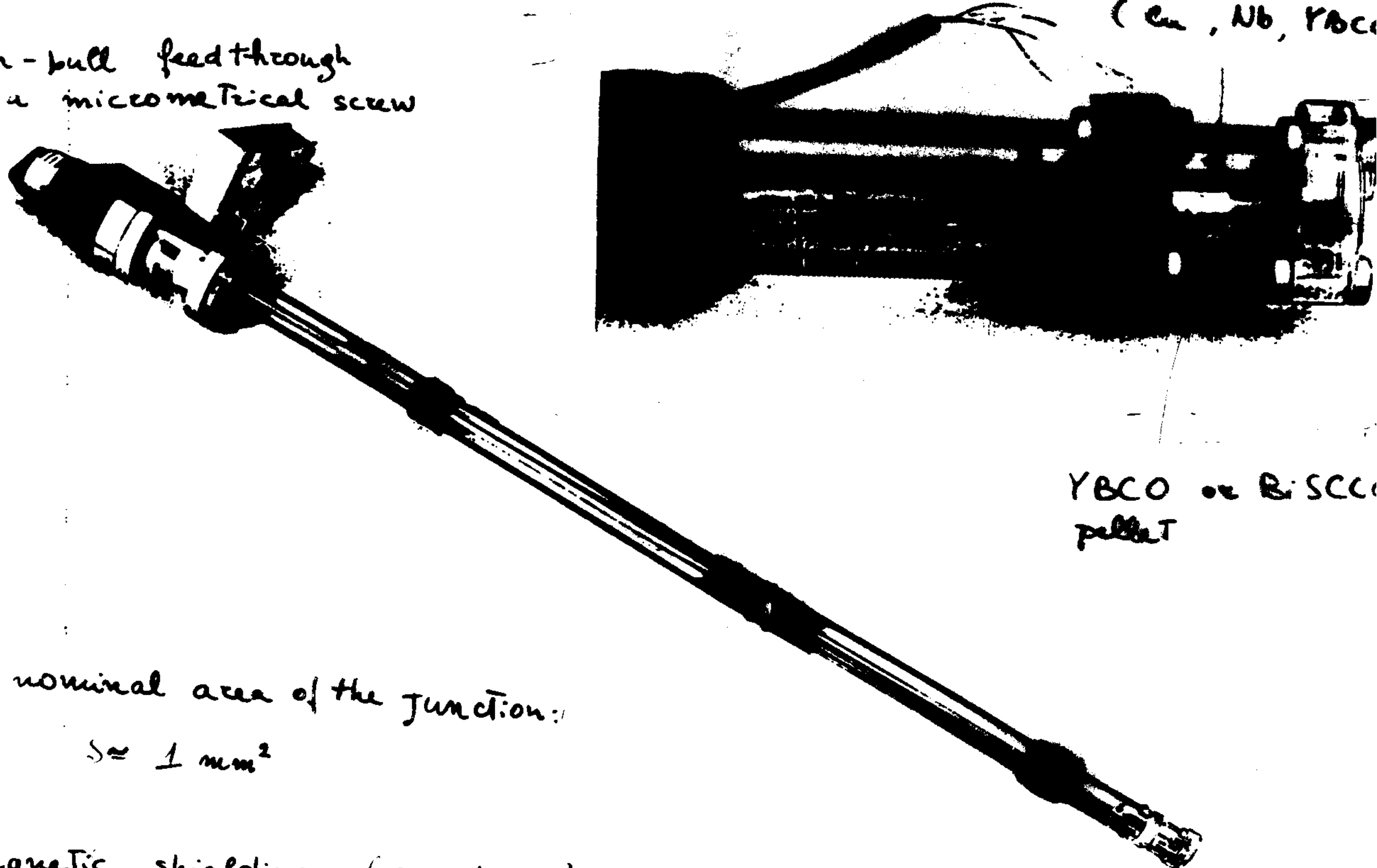

tip pressed on
the pellet
(Cu, Nb, YBCO

YBCO or BiSCCO
pellet

nominal area of the junction:

$S \simeq 1\ mm^2$

Magnetic shielding (cryoperm) is not shown
Thermal equilibrium is assured by a copper block and a suitable shield
Measurements are performed in ^4He vapours or in ^4He bath

A. Barone, A. Di Chiara, G. Peluso, U. Scotti di Uccio, A. M. Cucolo, R. Vaglio, F. C. Matacotta, E. Olzi

Phys. Rev B <u>36</u> 13 (1987)

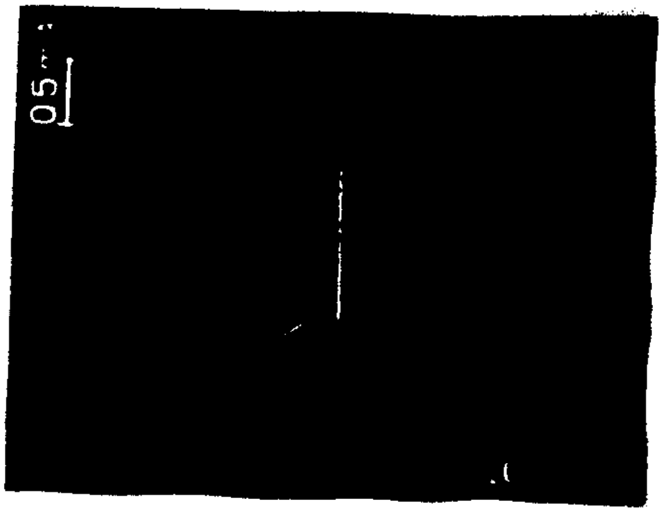

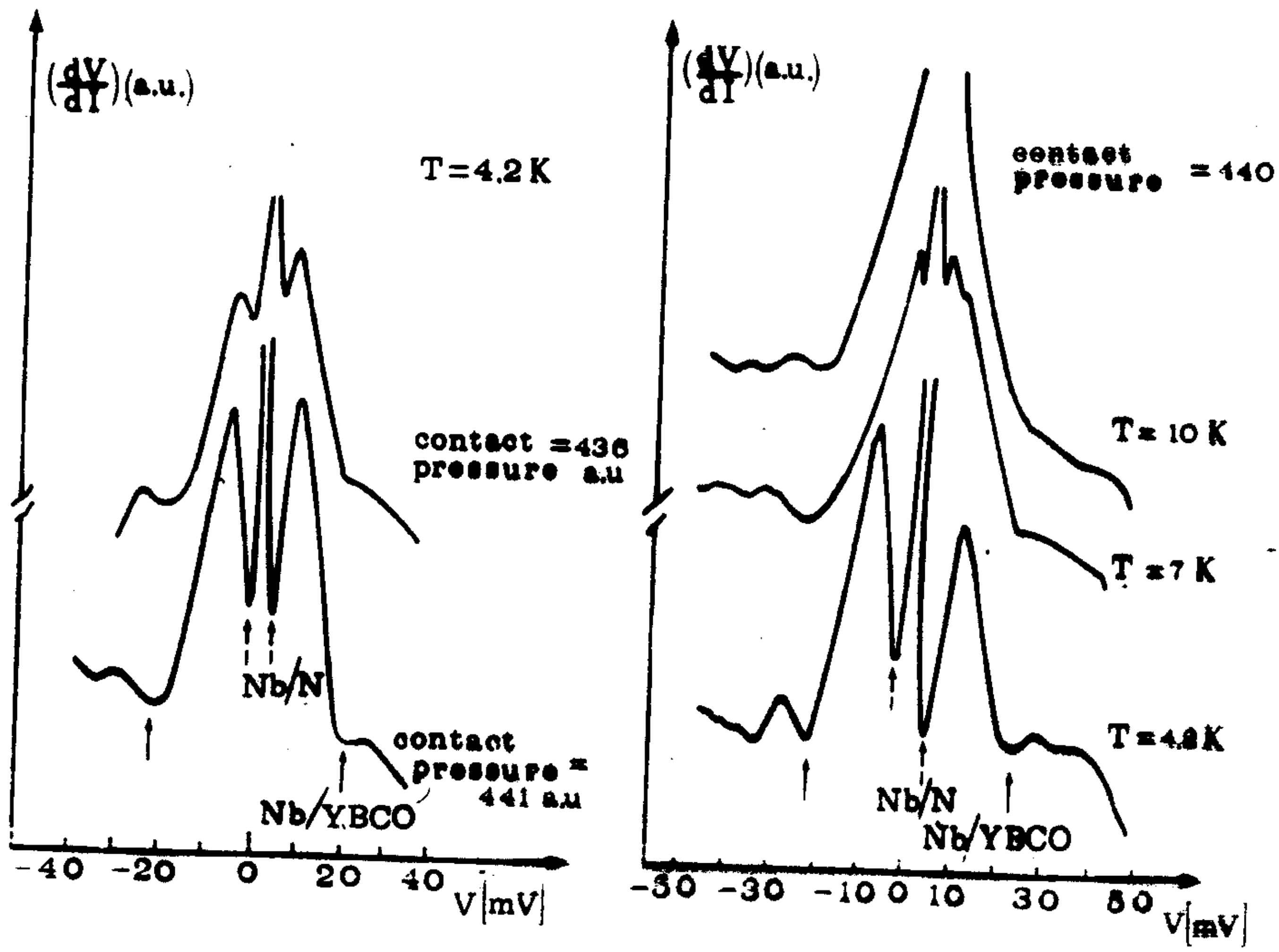

"Δ" = 19.5 ± 1.0 meV

$$\frac{2\Delta(0)}{KT_c} = 4.8 \pm 0.5$$

Bi SCCO

low contact pressure

(~1KΩ at 30mV)

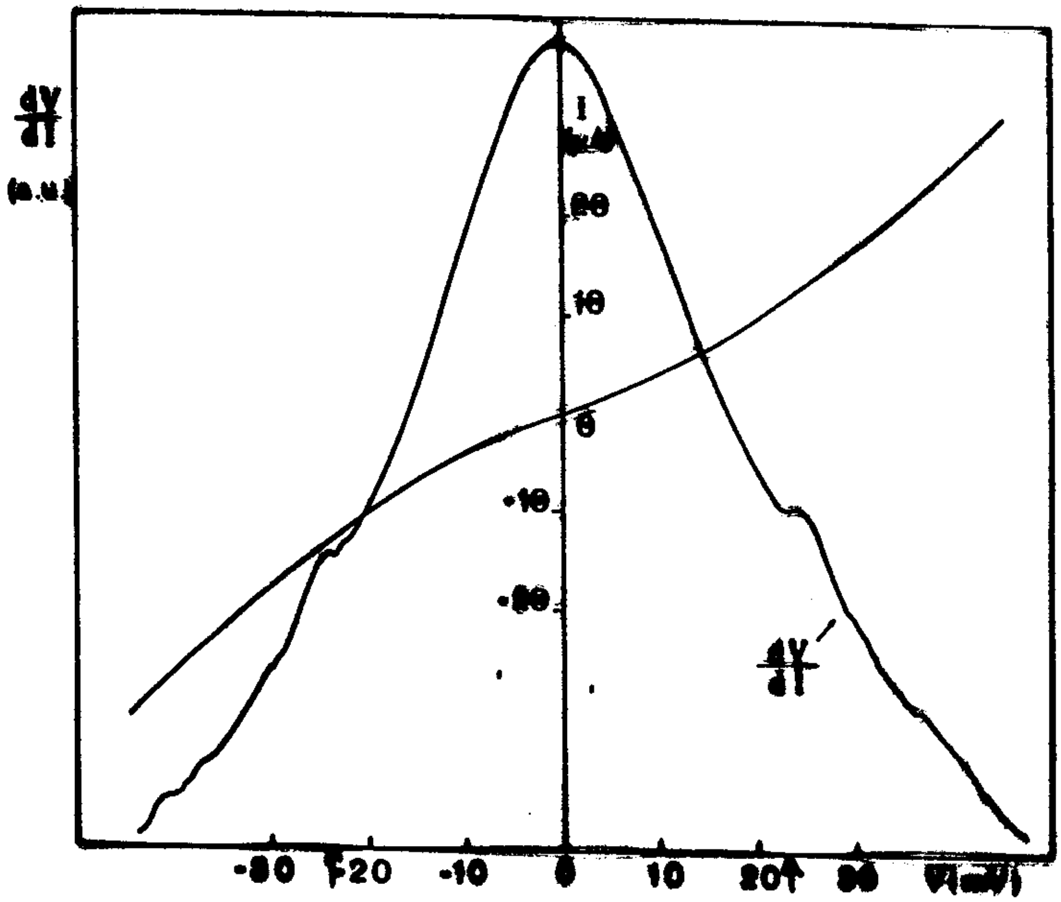

T = 14.2 K

$BiPbSrCaCu_2O_x$

June 1989

PR (to be published)

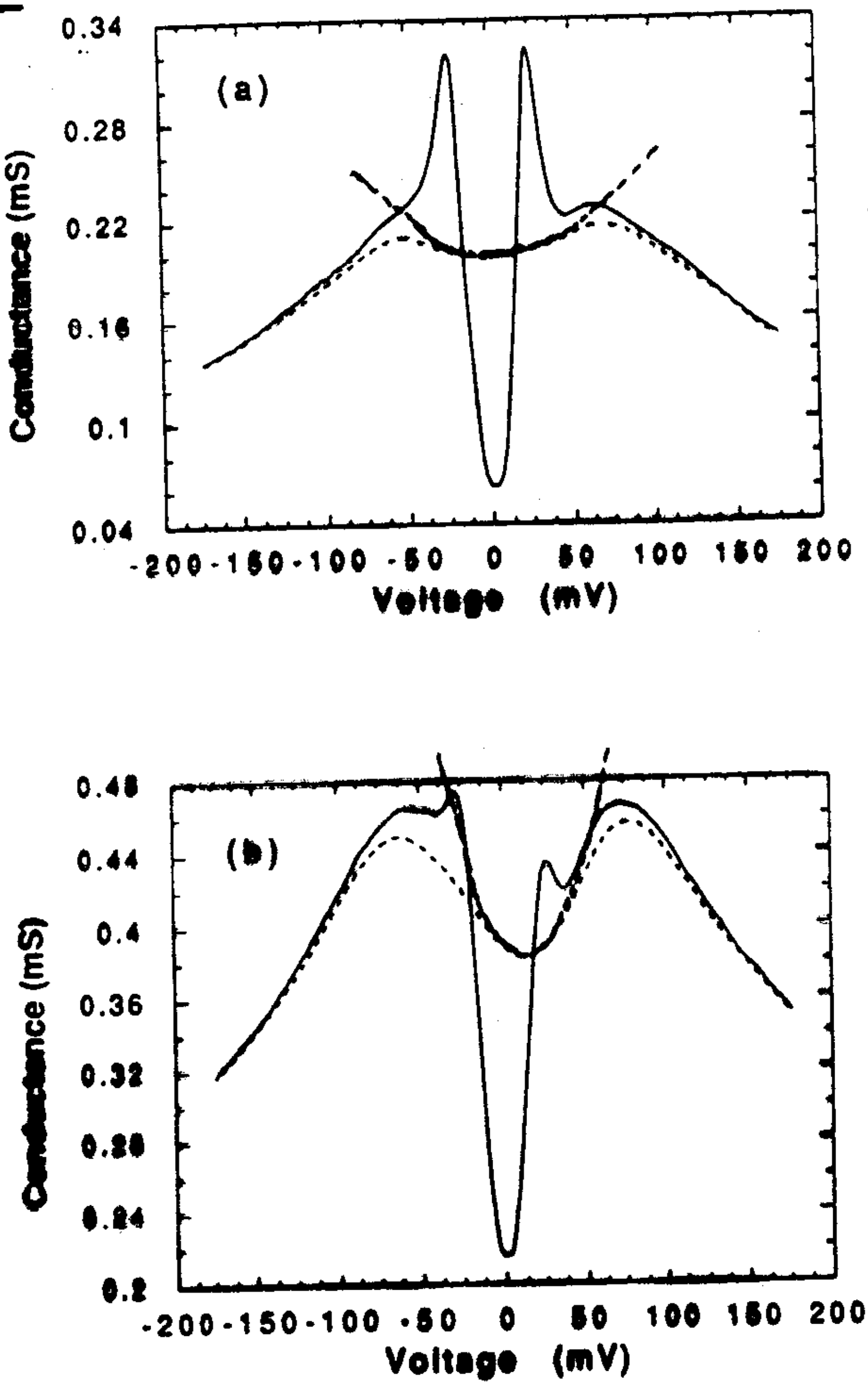

——— exp

- - - normal-state conductance fit for $|V| > 40$ mV

- - - Parabolic behavior due to $eV \gtrsim E_b$

Huang, [illegible] Univ. Illinois

Argonne

(to be published)

August 1989

$Tl_2Ba_2CaCu_2O_x$

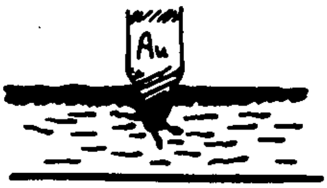

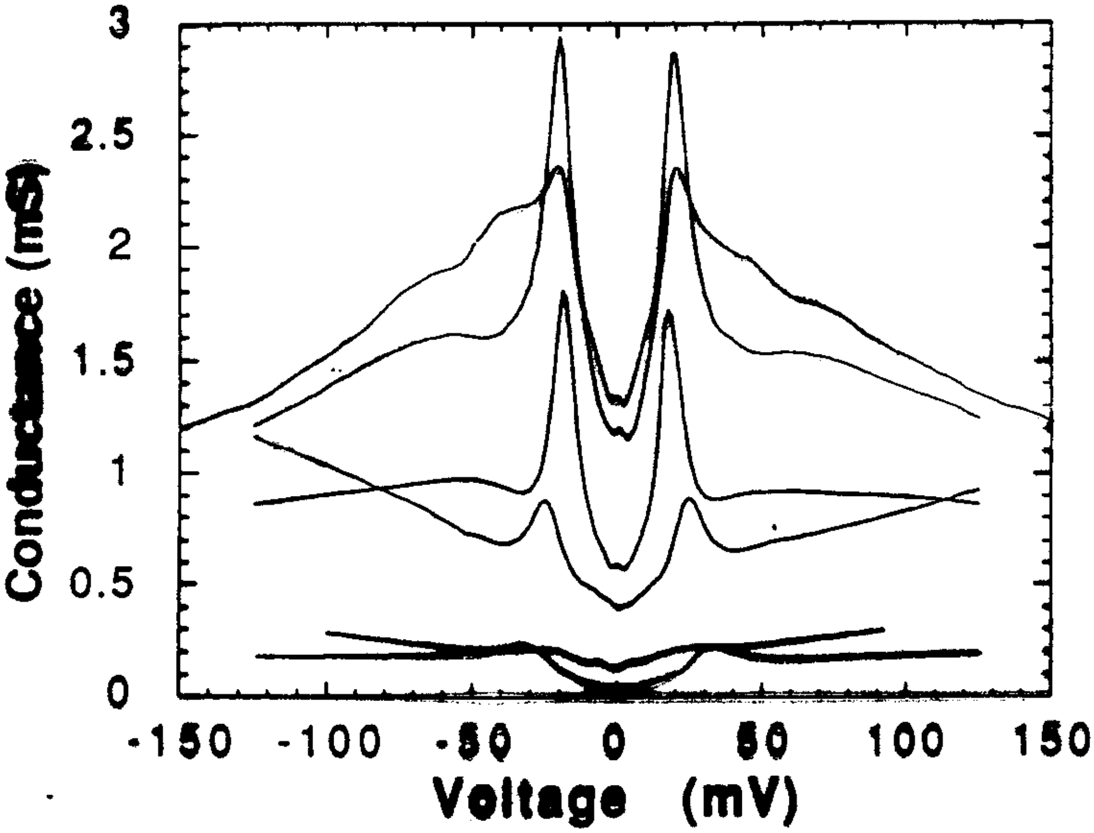

exp conductance for various R_n

mean grain size d ~ 1 μm

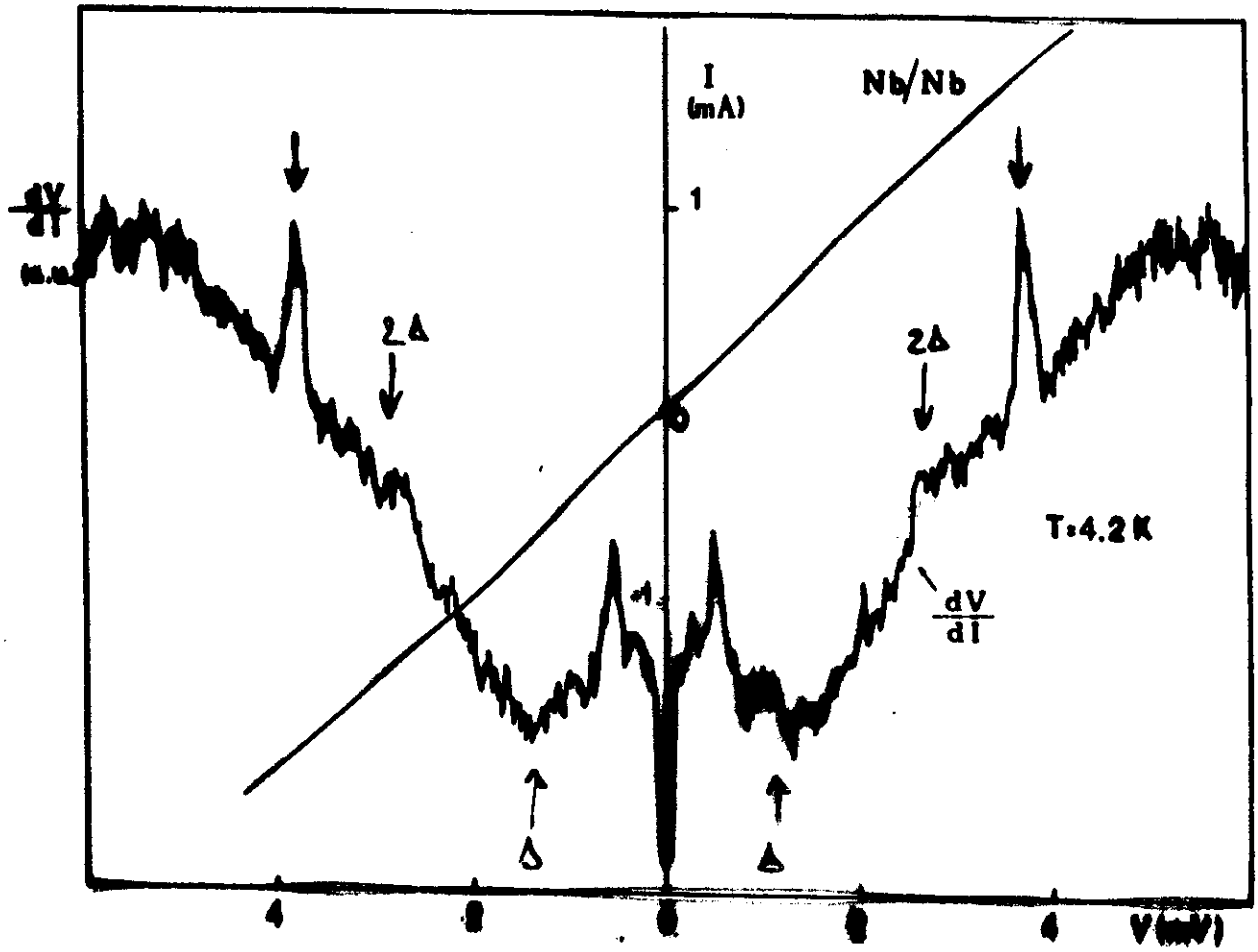

The overall aspect is dominated by a S-N PCJ and it is interpreted in the framework of the BTK theory for z<1 (low tunnel current).
The presence of structures at 2Δ ~ 2.5 mV indicates also the presence of S-I-S tunneling
The anomalous resistance peaks (blue arrows) are often observed in PCJ employing high Tc ceramics and are probably due to the granular nature of the sample.

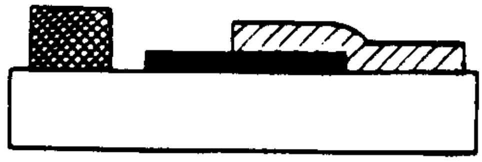

Fig. 1. – Sketch of the sample structure. The junction area (overlap geometry) is $(1 \div 2)$ mm^2. ▩ Cu, ☐ YBCO, ■ SiO, ■ Nb.

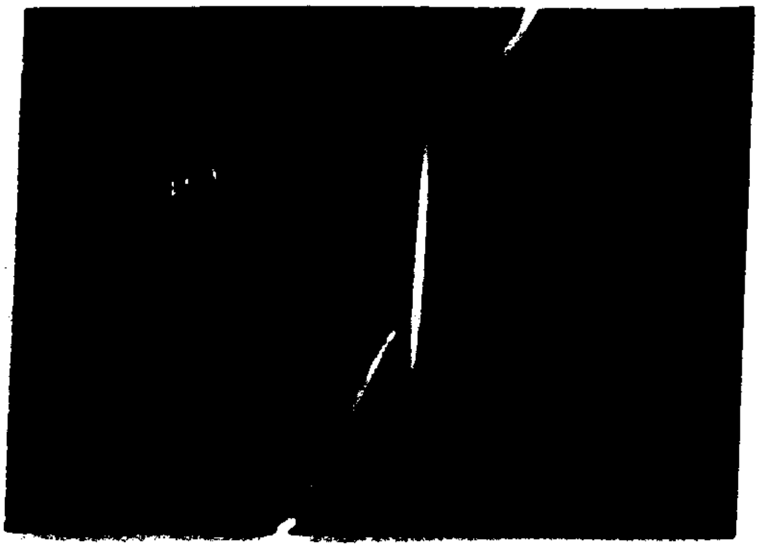

FIGURE 1
I-V characteristic at T=4.2K and H_e=0.

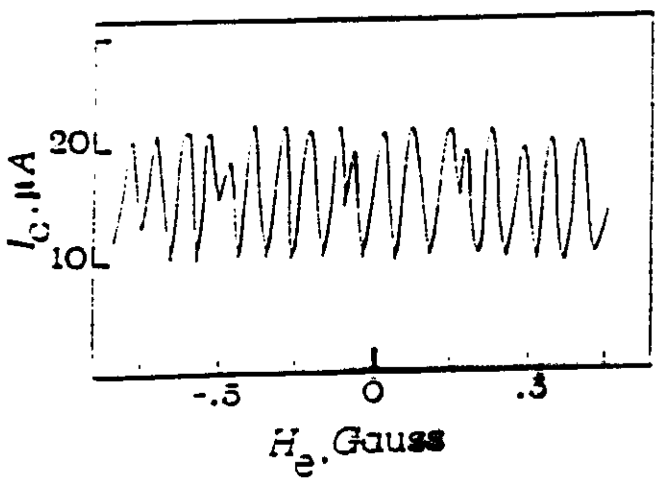

FIGURE 2
Maximum Josephson current vs. external magnetic field for an YBCO-Nb sample at T=4.2K.

High - T_c Superconductor FILMS

Deposition Techniques

Monotarget — single target of bulk material
difficulty of trasfering target stoichiometry to growing film

Sequential — deposition of the cation components from different target and subsequent ex-situ post annealing in oxygen

Co-Deposition Techniques

Magnetron Sputtering
Electron Beam coevaporation
Ion Beam Co-deposition
Laser ablation
Molecular Beam Epitexy

} flexible and controllable processes

SUBSTRATES

Quality of deposited films drastically dependent on crystallografy and preparation of substrates.

$SrTiO_3$ (100) highest current densities and film uniformity
Lattice parameter differs ~1% from that of $Y_1Ba_2Cu_3O_{6.9}$

$LaGaO_3$ recently discovered by IBM
(lattice mismatch ~0.5%)
favorable thermal expansion coeff. and better mechanical properties

YSZ
Yttrium stabilized Zirconia
lattice mismatch 30%

Si overlayed by ZrO_2 "buffer"

MgO
good results. mismatch ~ 8%

Silver layers, Sapphire substrates etc.

Important item is deposition Temperature
It should be minimized to avoid interdiffusion between YBCO and substrate

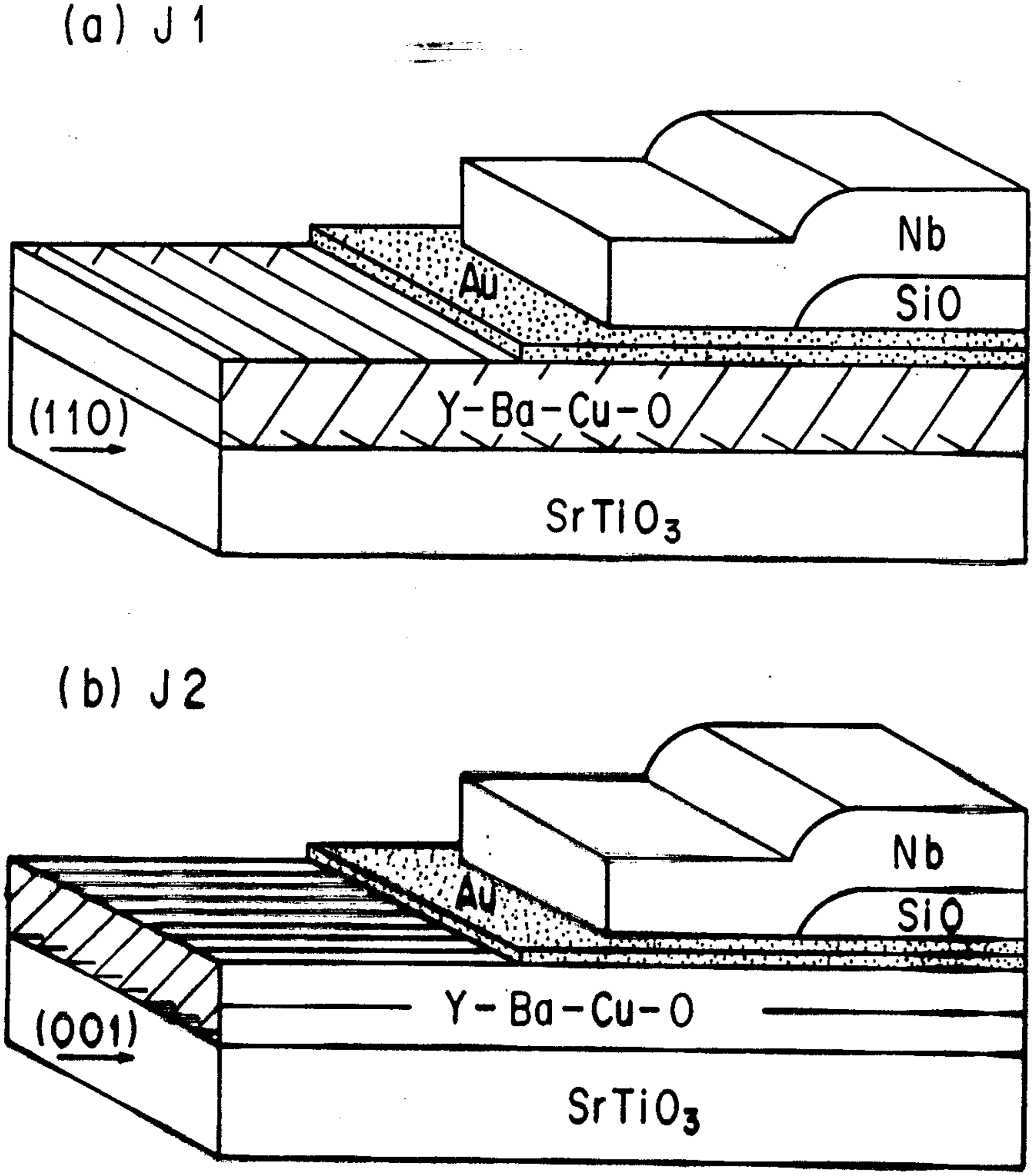
(a) J1
Nb
SiO
Au
(110)
Y-Ba-Cu-O
SrTiO3
(b) J2
Nb
SiO
Au
(001)
Y-Ba-Cu-O
SrTiO3

Akoh (1989) YBCO-Au-Nb

superconductively connected to the Nb film through the Au barrier due to the proximity effect. The normal resistance R_n is 0.48 mΩ, so that the $I_c R_n$ product is 13 μV. In order to verify the junction as a Josephson junction, a microwave was applied to the junction. Figure 2 shows the *I-V* characteristic of the junction under the microwave radiation with the frequency f of 9.216 GHz at 4.2 K. The critical current I_c is decreased to 18 mA under the microwave radiation. As is seen in the figure, the first harmonic step is observed at the voltage of $hf/2e$ due to the ac Josephson effect, where h is Planck's constant and e is the electronic charge. In addition, a subharmonic step appears at the voltage of $(1/2)(hf/2e)$.

Figure 3 shows the temperature dependence of the critical current I_c of the junction. I_c is proportional to $(1-T/T_{cj})$ near T_{cj}, where T_{cj} is the transition temperature of the junction. This linear temperature dependence of I_c suggests that the coherence length ξ_n of Au film is larger than the thickness of Au barrier [17].

Figure 4 shows the magnetic field dependence of the critical current I_c for the junction at 4.2 K, which exhibits the Fraunhofer pattern as observed in the Josephson junction. The magnetic field was applied parallel to the junction. This magnetic field dependence of I_c shows the behavior of the self-

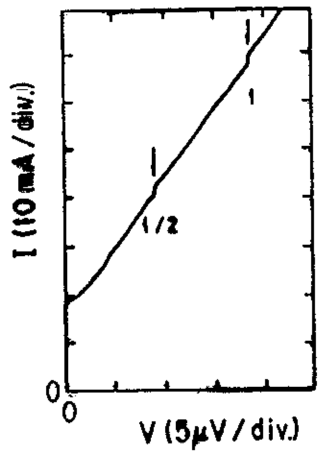

Fig. 2. *I-V* characteristic of *SNS* junction with polycrystalline Y-Ba-Cu-O film and a 30-nm Au barrier under a 9.216-GHz microwave radiation at 4.2 K.

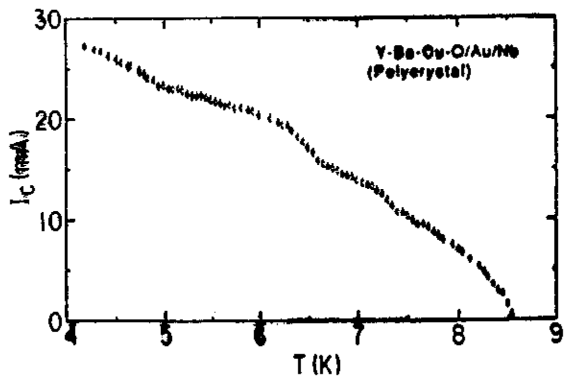

Fig. 3. Temperature dependence of critical current I_c for *SNS* junction with polycrystalline Y-Ba-Cu-O film and a 30-nm Au barrier.

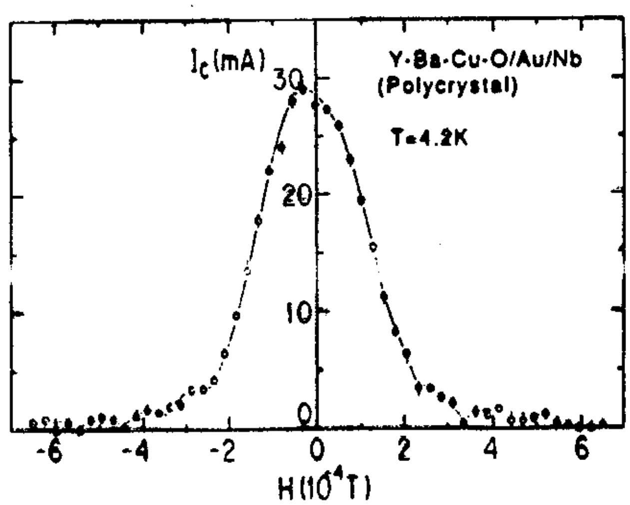

Fig. 4. Magnetic field dependence of critical current I_c for *SNS* junction with polycrystalline Y-Ba-Cu-O film and a 30-nm Au barrier at 4.2 K.

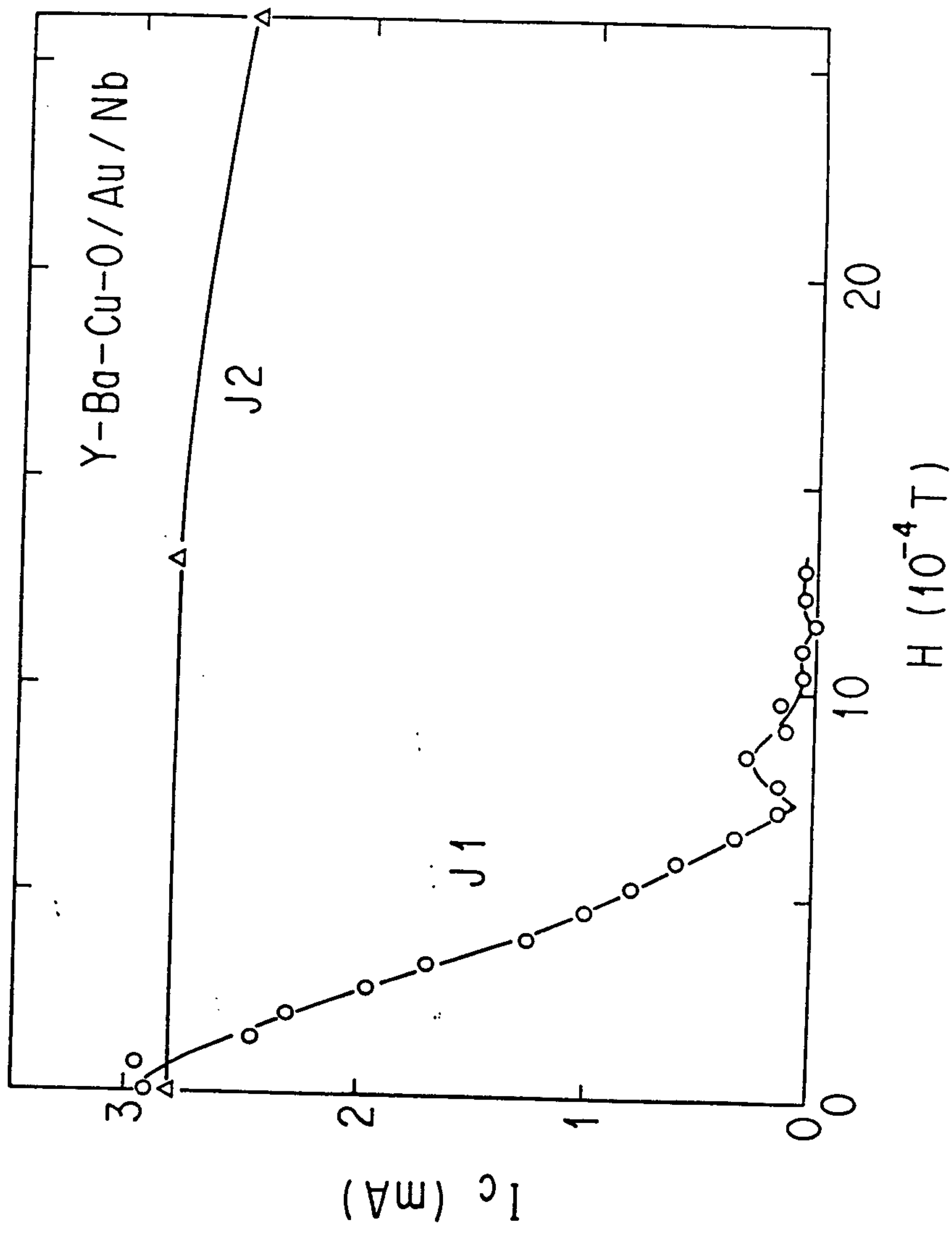
Y-Ba-Cu-O/Au/Nb
J2
J1
H (10^{-4} T)
I_c (mA)
0
10
20
0
1
2
3

(to be published)

Tunnel junctions on YBCO films

YBCO – Pb

4 samples of a single run

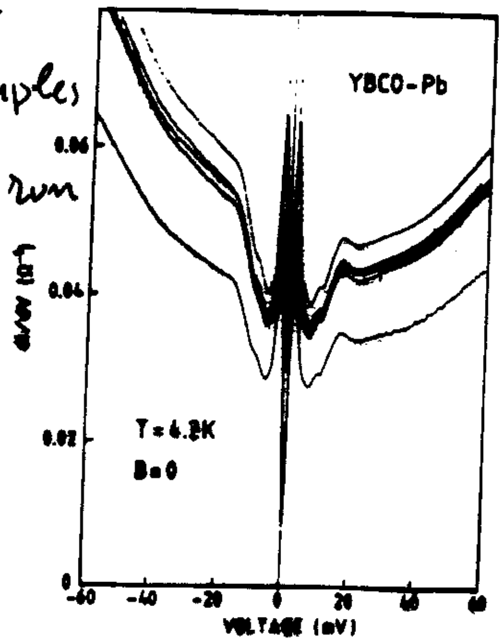

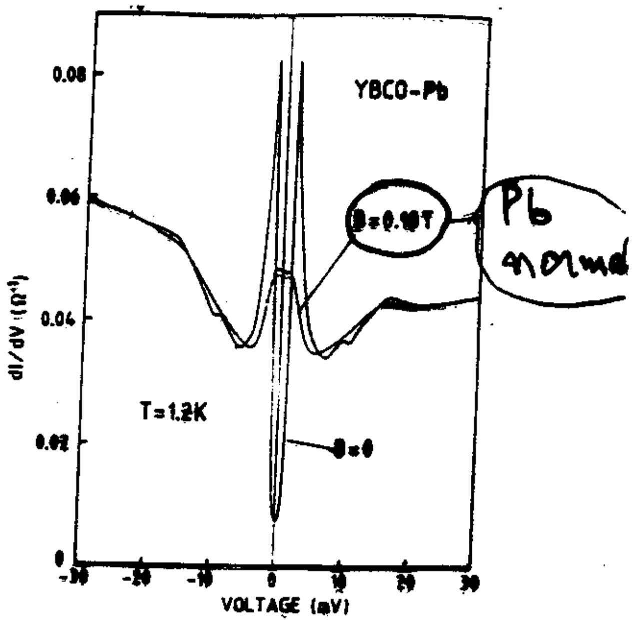

YBCO - In

10 samples of a single run

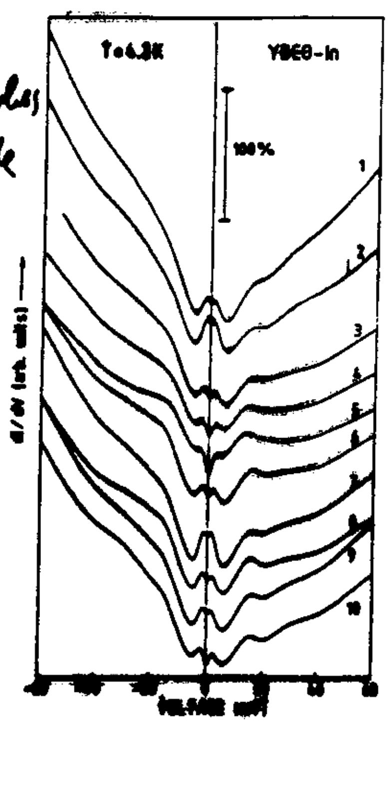

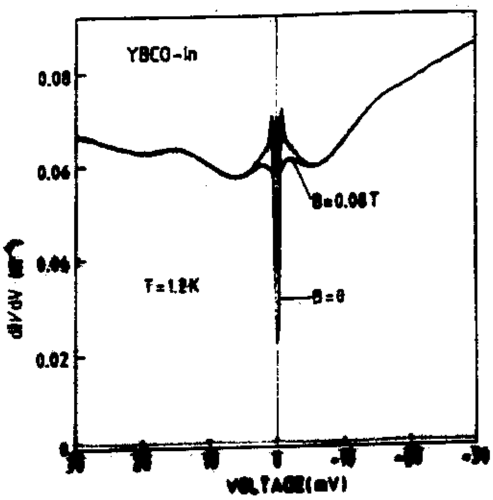

Thin films of YBCO epitaxially grown by magnetron sputtering on (100) and on (110) oriented $SrTiO_3$ substrates.

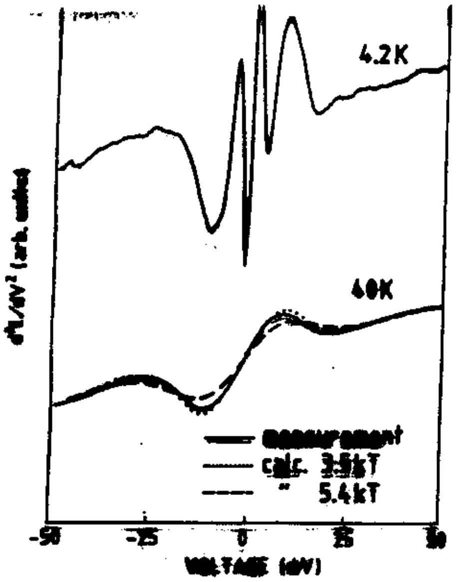

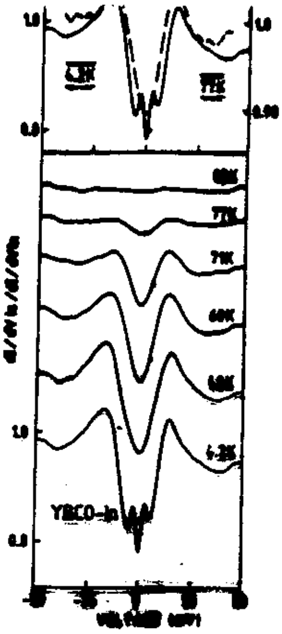

gap-like independent of T (?)

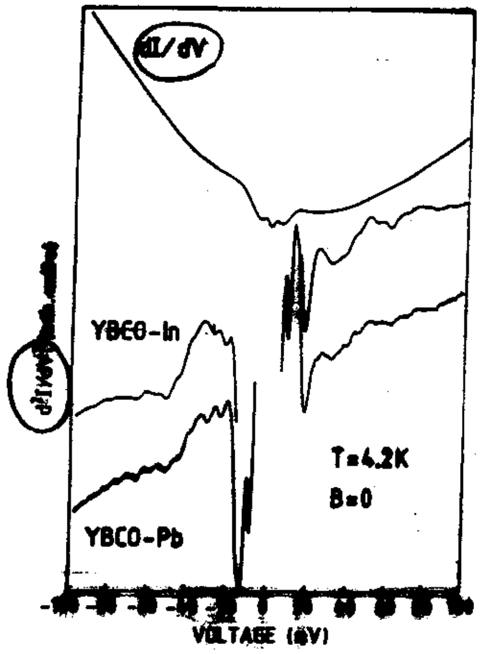

~> (parabolic)

~> (linear)

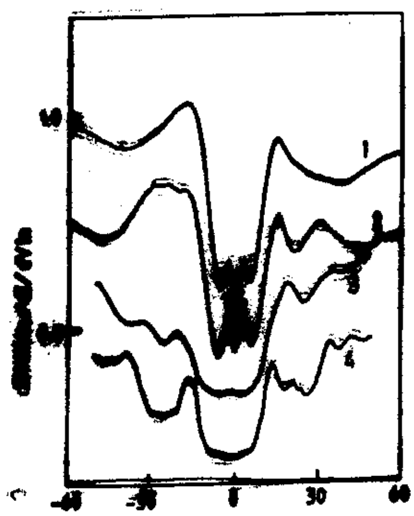

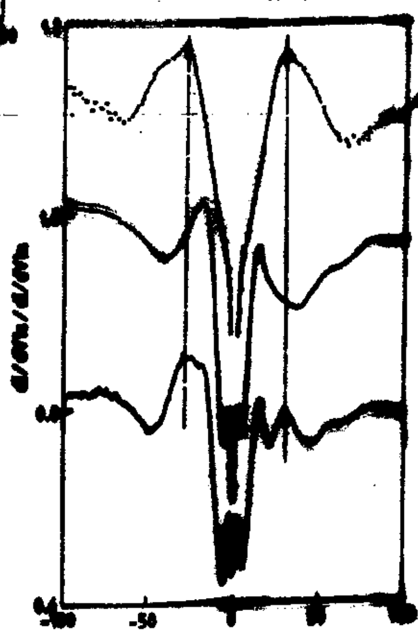

Fournel et al Europhys. Lett. in press (single crystal)

Geerk & Linker

Traces 1 and 2 Geerk & Linker
3 and 4 Kirtley et al. single crystal
H c //a,b

YBCO - Al - YBCO

S. Tanaka, H. Itozaki, S. Yazu ISS '89
Itami Res. Lab. Sumimoto Electric Industries

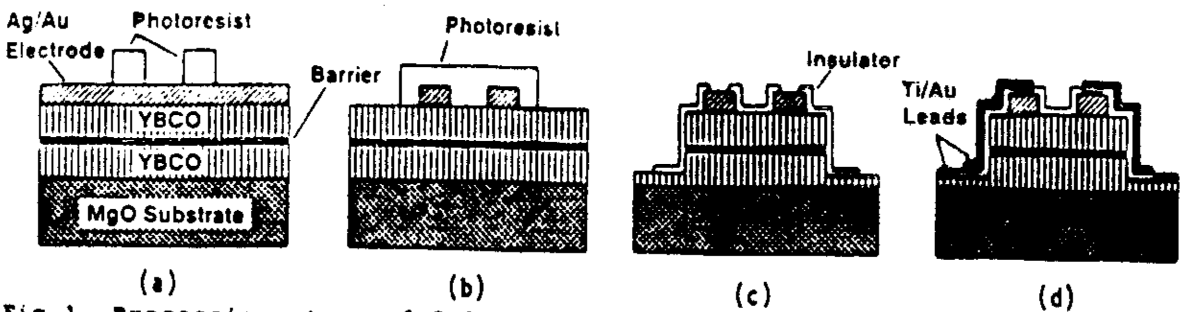

Fig.1. Processing steps of SNS junctions. (a) Formation of electrodes. (b) Definition of the junction area. (c) Ion beam etching and device isolation. (d) Formation of Ti/Au leads.

r.f. magnetron - ex situ technique

T = 18K

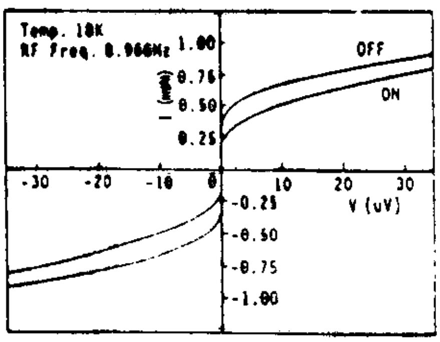

Fig.4. I-V characteristics of the device. Critical current Ic is suppressed under microwave irradiation.

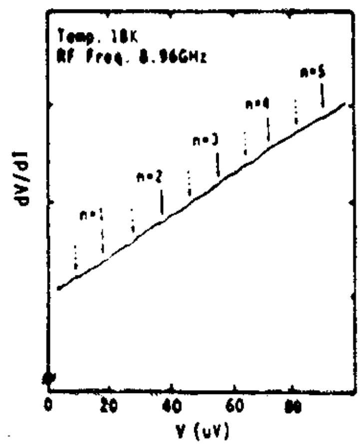

Fig.5. Differential resistance dV/dI as a function of voltage.

[illegible] et al. Jap. J. Appl. Phys. 27, L1107 (1988)

YBCO Bridge

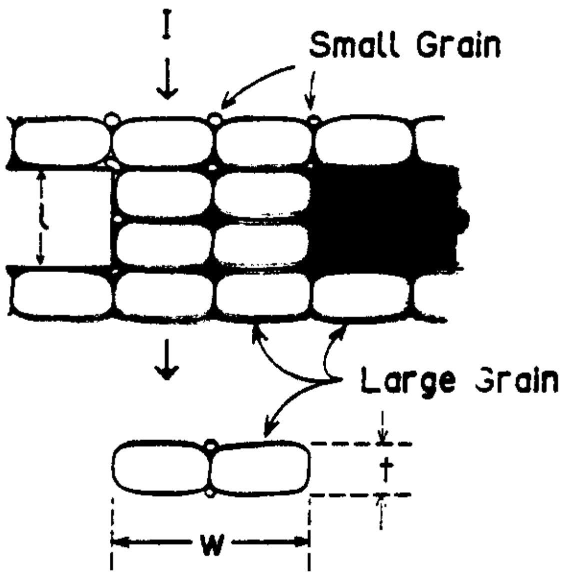

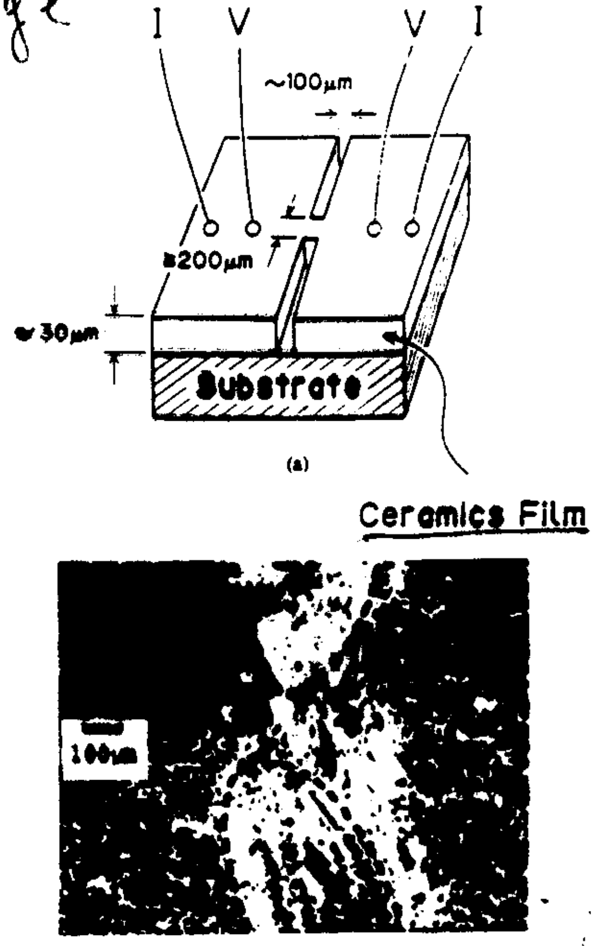

[illegible]

YBCO bridge

T = 77 K

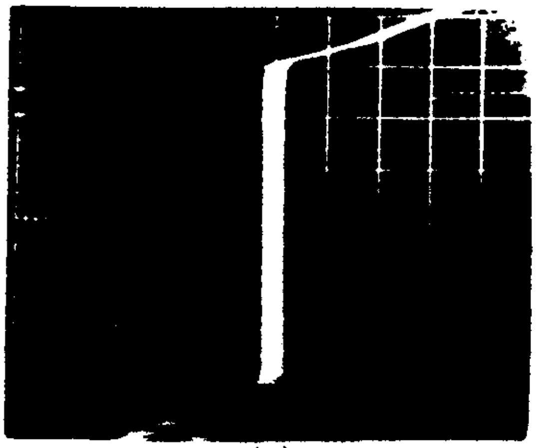

(a)

0.2 mA/div

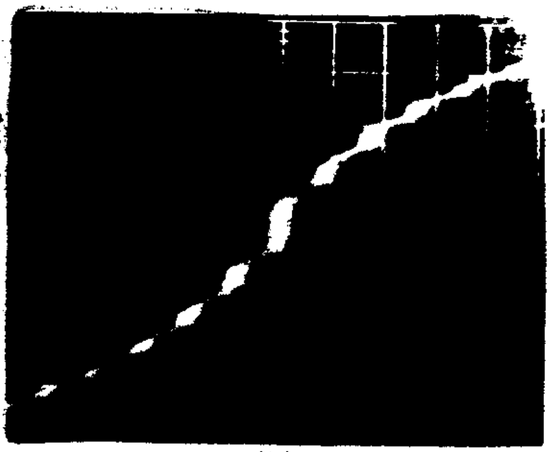

(b)

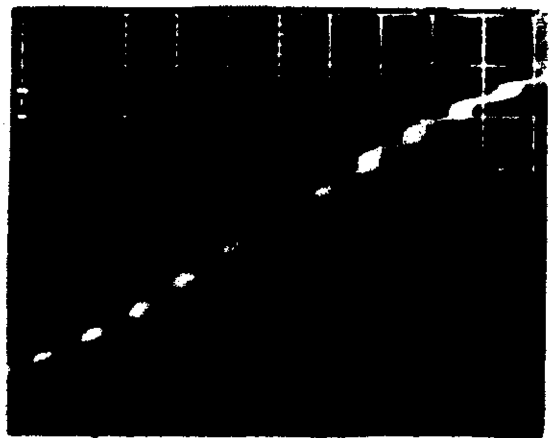

(c)

20 µV/div

8.2 GHz

Fig.17. The I-V curve of the bridge at 77K (a).
When 8.2 GHz is exposed to the bridge, clear Shapiro steps are observed (b) and (c). Power level is increased from (b) to (c).
X: 20 µV/div, Y: 0.2 mA/div. T=77K.

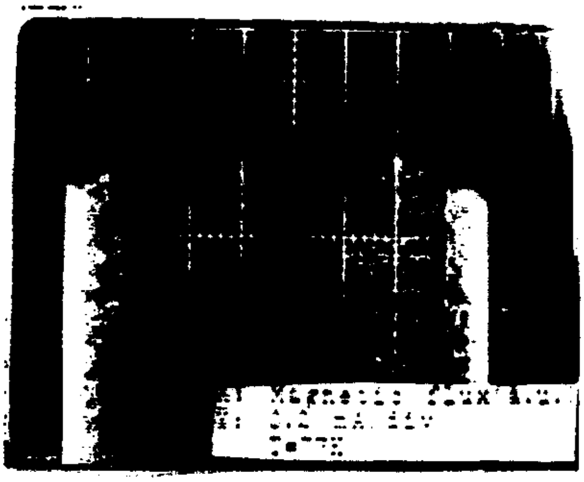

Fig.18. The magnetic field dependence of the critical current for the bridge at 77K.

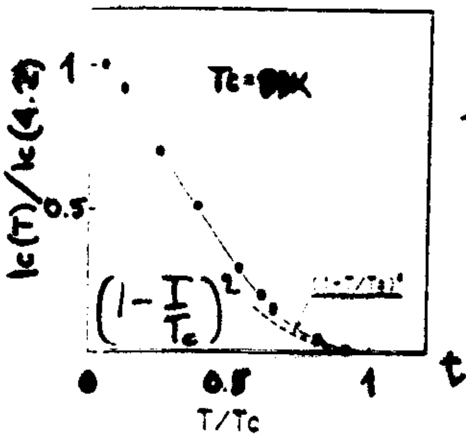

Tc = 89 K

Fig.19. The temperature dependence of the critical current for the bridge

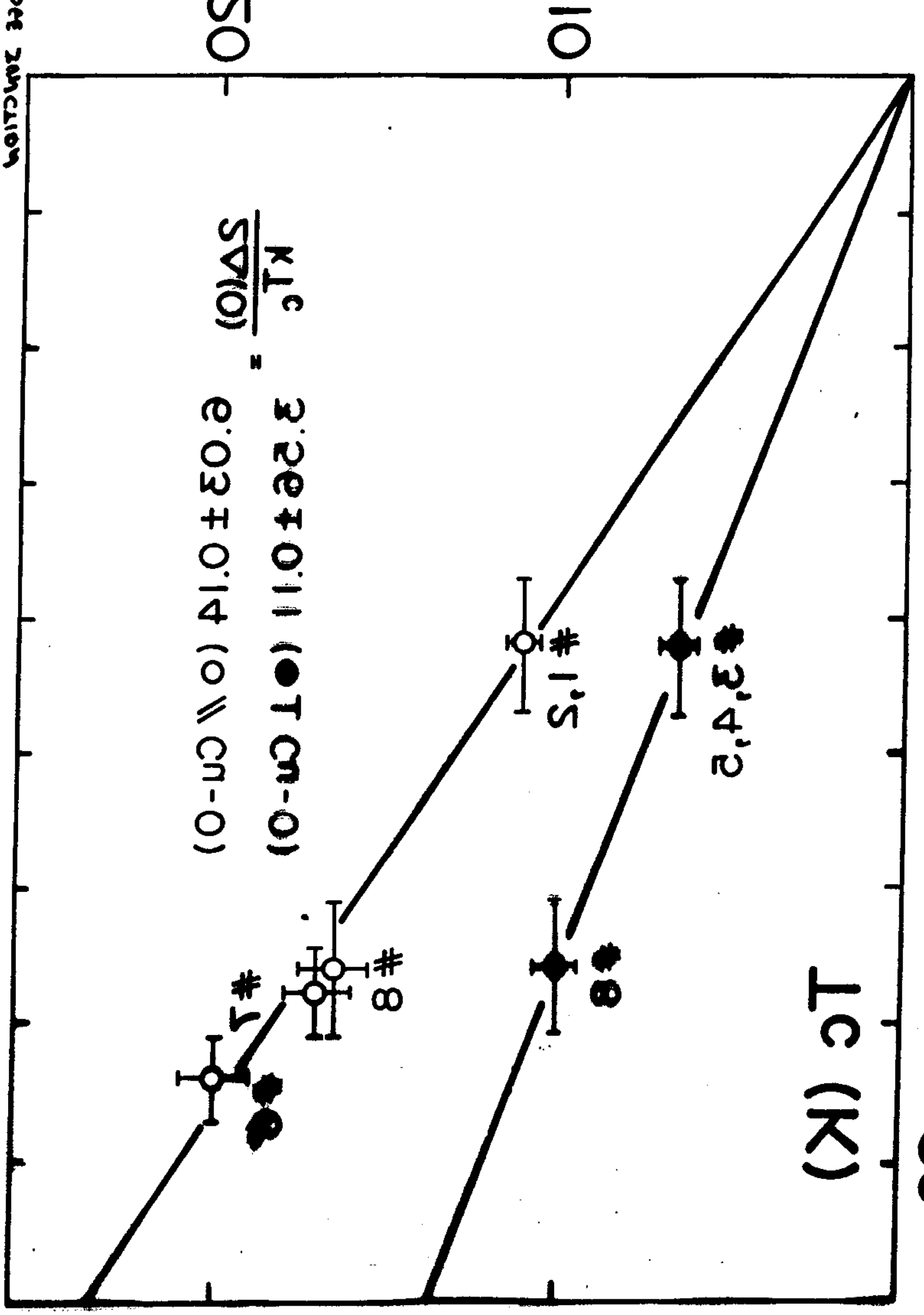

Tsai et al. Physica C 157, 533 (1989)

-15-

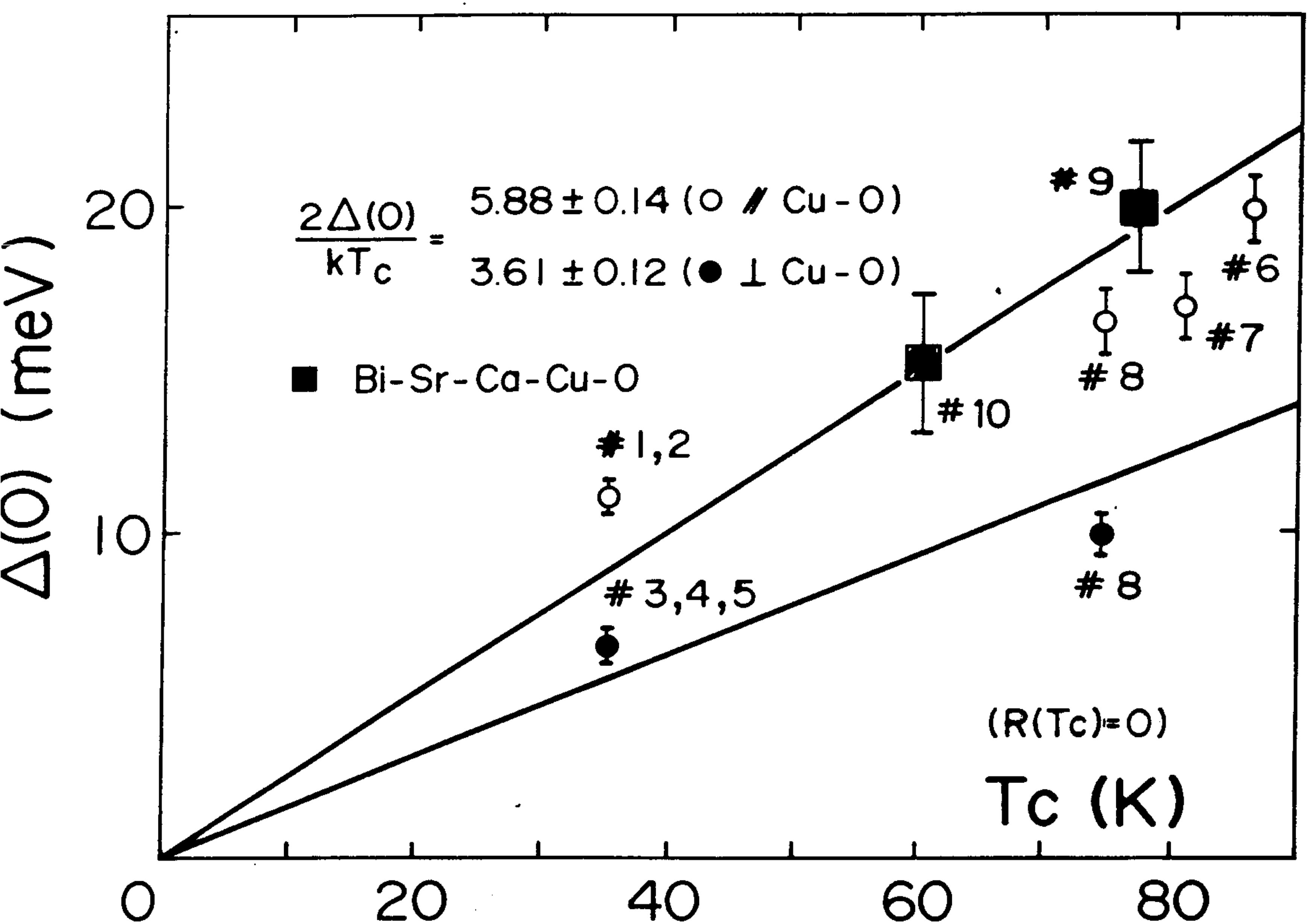
Δ(0) (meV)
20
10
0
20
40
60
80
2Δ(0) / kTc = 5.88 ± 0.14 (○ // Cu-O)
3.61 ± 0.12 (● ⊥ Cu-O)
Bi-Sr-Ca-Cu-O
#9
#6
#7
#8
#10
#1,2
#3,4,5
#8
(R(Tc)=0)
Tc (K)

15

44

Irie, Ere, Yamashita, Kurosawa, Yamane and Hirai (1989)

YBCO dc SQUID of MO-CVD Thin Film Bridge

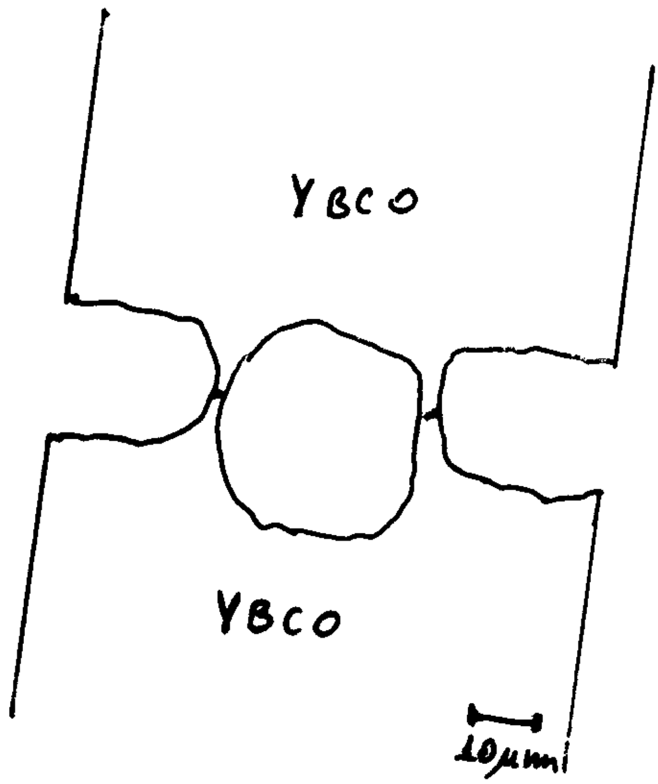

Energy Sens 740h @ 4.2K

Flux Noise 1.5 10^{-5} $\Phi_0/\sqrt{Hz}$

Table II Sputtering condition

Target	$Ba_{6.5}Y_1Cu_6$
Substrate Temp.	Room Temp.
Sputtering Gas	Ar
Gas Pressure	20 mTorr
Growth Rate	250 nm/hour

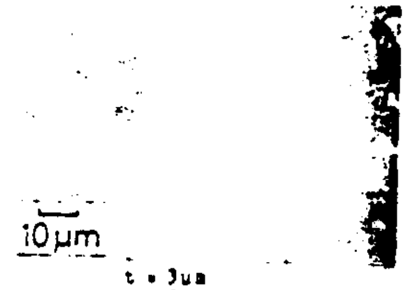

t = 3um
w = 5um
l = 10um

Fig.9. A SEM photograph of the weak link.

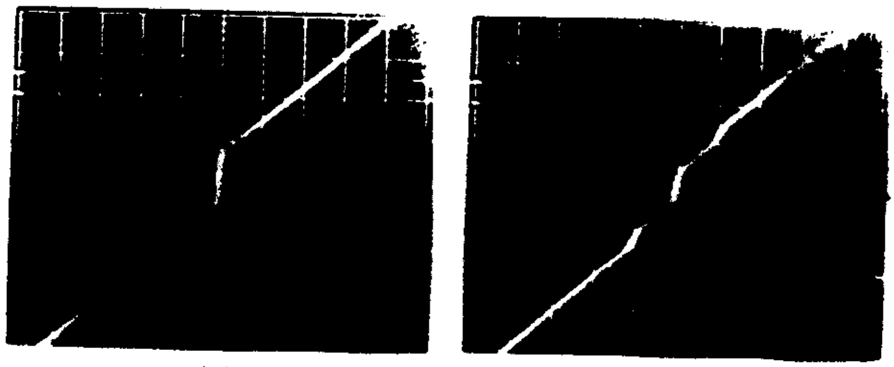

(a) (b)

Fig.10 The I-V curves of the device without rf radiation (a) and with radiation (b) of f=9.8 GHz at 70 K.
X:20 uV/div,Y:20 uA/div

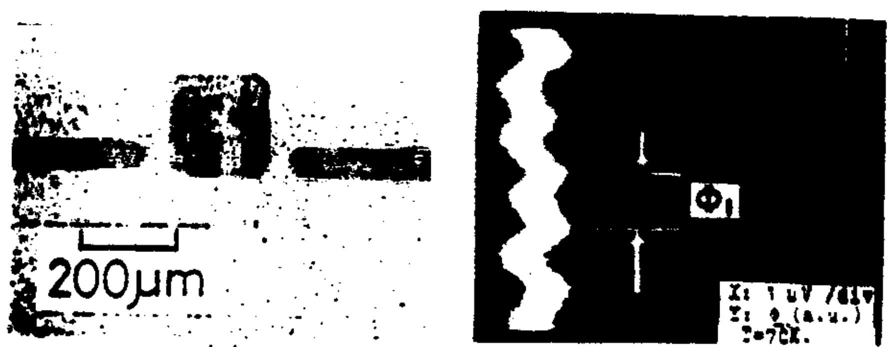

(a) (b)

Fig.11. The fabricated SQUID pattern (a) and V-Φ characteristics at 70 K (b).

Conclusions (!?)

- Tunneling Spectroscopy
  (identification of "Δ")
- Morphology vs. Physiology
  (granularity, layering)
- plane sandwich Junctions:

maybe we cant see ..... enough!

- point contact Junctions

maybe we can see ..... to much!

⇐/

Need for a S-I-S Tunnel Josephson J.

When?

When we shall have a surface "more rapresentative" of the material -

References and Suggested lectures:

A. Barone, G. Paternò
"Physics and Applications of the Josephson Effect"
J. Wiley New York 1982

K.K. Likharev
"Dynamics of Josephson Junctions and circuits"
Gordon and Breach Science Publ., N.Y. 1986

E.L. Wolf
"Principles of Electron Tunneling Spectroscopy"
Oxford University Press, Oxford 1985

L. Solymar
"Superconductive Tunneling and Applications"
Chapman and Hall LTD, London 1972